Journal of Alloys and Compounds 896 (2022) 163072

Contents lists available at ScienceDirect

Journal of Alloys and Compounds

journal homepage: www.elsevier.com/locate/jalcom

Review

Recent advances in Ti-6Al-4V additively manufactured by selective laser melting for biomedical implants: Prospect development

A.N. Aufa[a], Mohamad Zaki Hassan[a,*], Zarini Ismail[b]

[a] Razak Faculty of Technology and Informatics, Universiti Teknologi Malaysia, Jalan Sultan Yahya Petra, 54100 Kuala Lumpur, Malaysia
[b] Faculty of Medicine and Health Sciences, Universiti Sains Islam Malaysia, Bandar Baru Nilai, 71800 Nilai, Negeri Sembilan, Malaysia

ARTICLE INFO

Article history:
Received 21 September 2021
Received in revised form 27 November 2021
Accepted 29 November 2021
Available online 3 December 2021

Keywords:
Selective laser melting
Ti-6Al-4V
Stress shielding effect
Chemical treatment
Surface coating
Osseointegration

ABSTRACT

Recently, additive manufacturing (AM), being part of IR4.0, received great attention for the fabrication of customized implants with outstanding quality, which are used in hard tissue replacement. For an orthopedic application, the titanium alloy implants, especially those that use Ti-6Al-4V manufactured by selective laser melting (SLM), should facilitate maximum osteointegration between the implant and corresponding bone. However, the superior mechanical characteristics, poor surface integration, antibacterial performance, and readiness of SLM Ti-6Al-4V for use in advanced implants are still not comparable to those of anatomical bone. This review focused on the current issue of stress-shielding limitations in SLM Ti-6Al-4V owing to failures in load-bearing applications. The surface treatment and modification strategy that might improve the osseointegration of the implant were discussed. The corrosion resistance of SLM Ti-6Al-4V which could significantly affect antibacterial capability, improve cell adherence and apatite formation on the bone remodeling surface was also addressed. Finally, the current challenges, prospects and applications for SLM Ti-6Al-4V development were presented.

© 2021 Elsevier B.V. All rights reserved.

Contents

1. Introduction . . . 1
2. Selective laser melting (SLM) . . . 3
3. Stress-shielding effect of SLM Ti-6Al-4V implants . . . 5
4. Surface treatment of Ti-6Al-4V biomedical implant . . . 11
5. Surface modification of SLM Ti-6Al-4V . . . 12
6. Corrosion resistance of SLM Ti-6Al-4V . . . 16
7. Challenges and the way forward . . . 17
   7.1. Cavity size manufactured by using SLM and biomedical needs . . . 18
   7.2. SLM Ti-6Al-4V structures with bioactive surfaces . . . 18
   7.3. Novel β-titanium alloys for lattice implants . . . 18
8. Applications of SLM Ti-6Al-4V . . . 18
9. Conclusions . . . 20
Declaration of Competing Interest . . . 20
Acknowledgments . . . 20
References . . . 20

1. Introduction

The human skeleton is a dynamic support structure that consists of 206–213 bones in adults. It provides the reinforcement structural support system that gives the human body its shape, allows

* Corresponding author.
E-mail address: mzaki.kl@utm.my (M.Z. Hassan).

https://doi.org/10.1016/j.jallcom.2021.163072
0925-8388/© 2021 Elsevier B.V. All rights reserved.

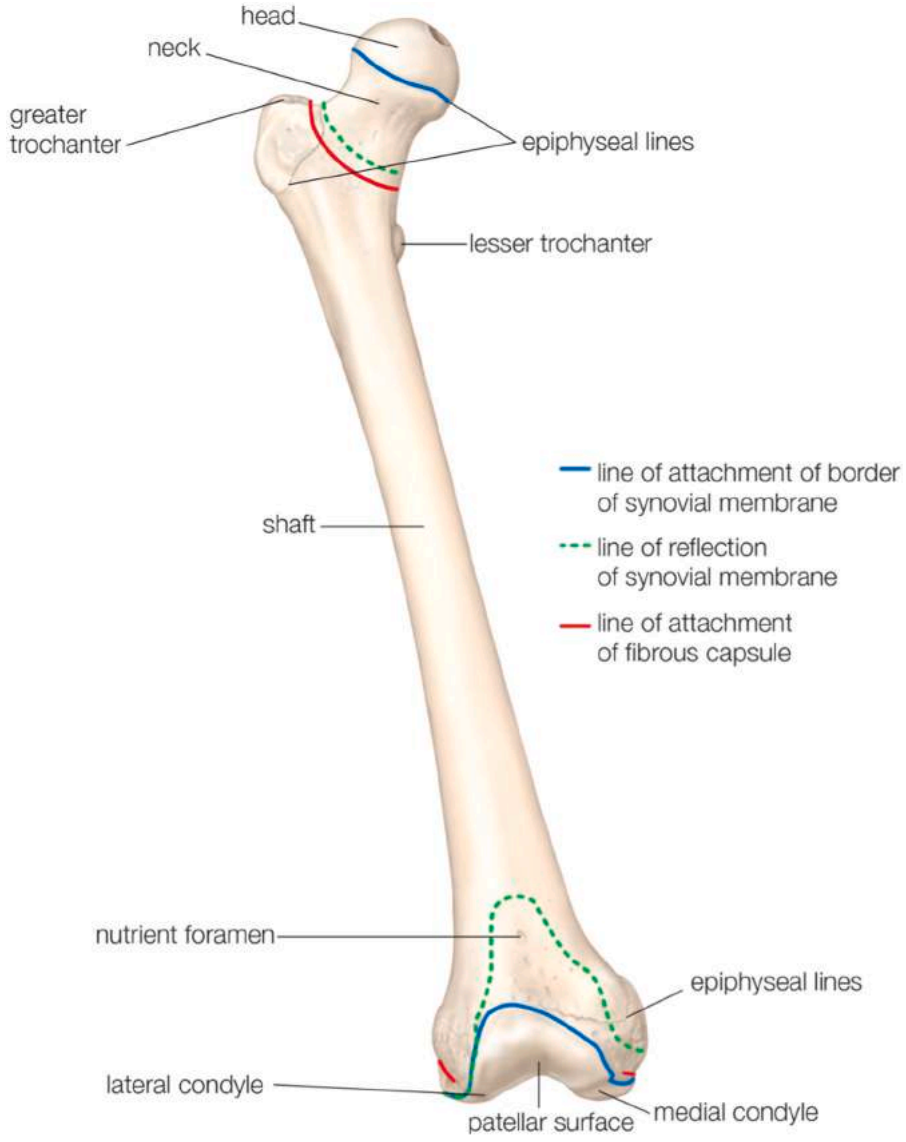

Fig. 1. Anatomic structure of human bone [208].

locomotion, facilitates respiration, enables breathing and protects vital organs. It also plays a significant role in homeostasis [1]. Furthermore, bones have a role in the production of red-white blood cells, platelets, and the storage of minerals such as calcium, magnesium, and phosphorus. Bone tissue is continually changing, being restructured and biologically remodeled throughout life [2]. Many different bone cells such as osteoprogenitor cells, osteoblasts, osteoclasts, and osteocytes are constantly reshaping throughout growth. Some involuntary muscles are attached to the bone tissue that contract and relax thereby pulling the structure to enable functional movement. Fig. 1 shows the three typical major parts of the structural bones [3]. The epiphyses and metaphysis bone are generally prone to fracture as they are made of spongy osseous. Both are less resistant to stress as compared to dense diaphysis compact bone [4]. The epiphyseal plate, also known as hyaline cartilage, is located at the epiphysis of long bone and acts as a growth plate [5]. It pushes outward until longitudinal development ends due to the maturation of cells. The metaphysis-epiphysial line is brittle and can easily rupture as a consequence of injury or a fall. Once fracture occurs, the periosteum will release the osteoblasts to build a new bone. Then, it remodels the bone to form a hard tissue at the fracture gap. As can be seen from Fig. 1, the medullary cavity inside the diaphysis bone shaft plays an important role in generating red blood cells carried by the nutrient artery to foster the healing process [6]. To improve bone healing after fracture, orthopedic implantation is used to restore the anatomical function of the damaged structure [7,8]. The fracture healing of cancellous bone is shorter than for cortical bone because it is less dense, more elastic, and has higher porosity [9,10].

In the early 1950 s, Branemark firstly defined the term osseointegration as "the bonding of human bone cells to the metallic surface of implants". In this study, a titanium implant was used to fix artificial teeth into the jaw and effectively, osseointegration occurs in the human body. These devices showed outstanding characteristics, including excellent material characteristics, high corrosion resistance and biocompatibility when implanted [11].

The open reduction internal fixation (ORIF) depends on fracture sites, and thus different implants were developed by to enhance the function of body parts [12,13]. This technology permits early patient mobilization and prevent joint stiffness and deformity [14,15]. However, unsuccessful osseointegration may cause strain at the fracture healing site. It also increases the risk of tears in the repaired tissue, which hasten the removal of the implant and predominantly lead to infection in the patient [16,17]. Based on these considerations, cobalt-chromium-based alloys,

Table 1
The tensile and compressive properties of materials developed for orthopedic implantation.

Materials	Benefit	Drawback	Biomedical applications	Tensile strength (MPa)	Tensile modulus (GPa)	Compressive strength (MPa)	Compressive modulus (GPa)	Ref
Skeletal (Cortical)				70–150	15–30	90–209	17–20	[16,17,102]
Skeletal (Cancellous)					4–30	7.36 – 8	0.2–2	
316 L Stainless Steel	Low-priced, readily accessible, good biocompatibility, can cause an allergic reaction.	High modulus, poor resistance to corrosion, can cause an allergic reaction.	Fracture plates and screw, Ilizarov frames.	490–1350	200–210	70	193	[16,204]
Chromium Based Alloys	Higher oxidation and corrosion resistance, fatigue strength.	Expensive, high modulus.	Total hip replacement, k wire fixation and bone plates.	655–1793	210–253	196	190–210	[16]
Titanium-based Alloys	MRI-compatible, corrosion-resistant, lightweight, lower modulus.	Low wear resistance.	Total Hip replacement, fracture fixation elements (Illizarov frames, plates, screws)	690–1100	110–114	1000	45	[16,17]
Dense HA ceramics			Coating on surface of an implant.	40–100	70–120	430–920		[205]
Bioglass 4555				42	35	0.2–0.4	500	[206,207]

stainless steel, and titanium and its alloys are amongst the commonly used materials for metal implants [16,18].

Table 1 shows the properties of typical orthopedic implants currently available in the market as compared to the human bone. As can be seen from the table, metallic materials are predominantly utilized to fix fractures and deal with bone distortion. Even though 316L stainless steel is inexpensive, has a high modulus of elasticity and can construct stable fixation as compared to Ti and Co-Cr, it is less preferred by surgeons for long term fixations since it is also non-MRI (Magnetic Resonance Imaging) compatible and prone to infections after fixation [19,20]. Therefore, the most commonly non-metallic material utilized in clinical applications is hydroxyapatite (HA) and bioglass 45S5 [21,22], which are bioceramics that easily bond with a skeleton since they have the same crystalline structure as the human bone [23]. However, they cannot provide the load-bearing capability in the harsh microenvironment of the human body during functional movement of bone systems as they are brittle and easily broken [24].

In contrast, titanium-based alloys have the highest yield strength and can easily distribute stress at adjacent bone tissues, making them the most attractive implant materials. These alloys are available in three forms: alpha (α), beta (β), and alpha + beta (α + β). α alloys can be divided into (α) and 'near (α)' phase groups [25,26]. Both kinds of alloy are corrosion resistant and weldable. Since 1950, the (α) phase has been a pioneer in biomedical implants due to its pure Ti (Cp-Ti) composition. Nevertheless, at room temperature, it has a significantly low tensile strength (240–480 MPa) and an elastic modulus of 105 GPa as compared to (α + β) type alloys. This low tensile strength of alloys makes them unsuitable for use in load-bearing applications and it contributes to implant slackening [27,28]. Therefore, this material is only suitable for use in elevated-temperature applications (up to 500 °C) in the space industry [29].

The (α + β)-type Ti alloys consist of near α phase and minor β phase compositions. Amongst those, Ti-6Al-4V is the most widely used in traumatology implants as it prioritizes good fabricability, including high yield strength at room temperature. It provides rapid osseointegration by progressively producing a TiO_2/OH film on the bone surface besides triggering cell adhesion after implantation [30].

To date, some technological advances in the manufacturing of Ti-6Al-4V for biomedical applications have begun to emerge, such as alloy steel welding, metal injection molding and 3D printing. Additive manufacturing (AM) is a hybridized production technique for Ti-6Al-4V parts which has the advantages of shorter manufacturing time, higher material accessibility, and fabricability compared to the commercially distributed implants in the market [31,32]. In 2012, Dr Jules Poukens pioneered an additive engineered skull implant for a patient in Belgium, which offered a robust muscle attachment in addition to ample room for nerves [29].

This study's objective is used to serve as a fabrication guide for Ti-6Al-4V by using selective laser melting (SLM) for biomedical applications. Initially, method to reduce the stress shielding effect by following the surface treatment of SLM Ti-6Al-4V for implants was discovered. The effect of surface modification of SLM Ti-6Al-4V as a technique to improve tissue integration and avoid any deleterious cytotoxic consequences was also examined. Then, ways to improve the corrosion resistance were also discussed. Future directions and application of SLM Ti-6Al-4V in biomedicine were explained.

2. Selective laser melting (SLM)

The increasing need for complex-shaped, high-quality components and reduction of product waste has prompted the advancement of additive manufacturing (AM), also known as three-dimensional (3D) printing, as a manufacturing technology since the mid-1980 s [33,34]. AM is generally described as a layer-by-layer deposition to build a dense 3D product by using a digitally tuneable material laying

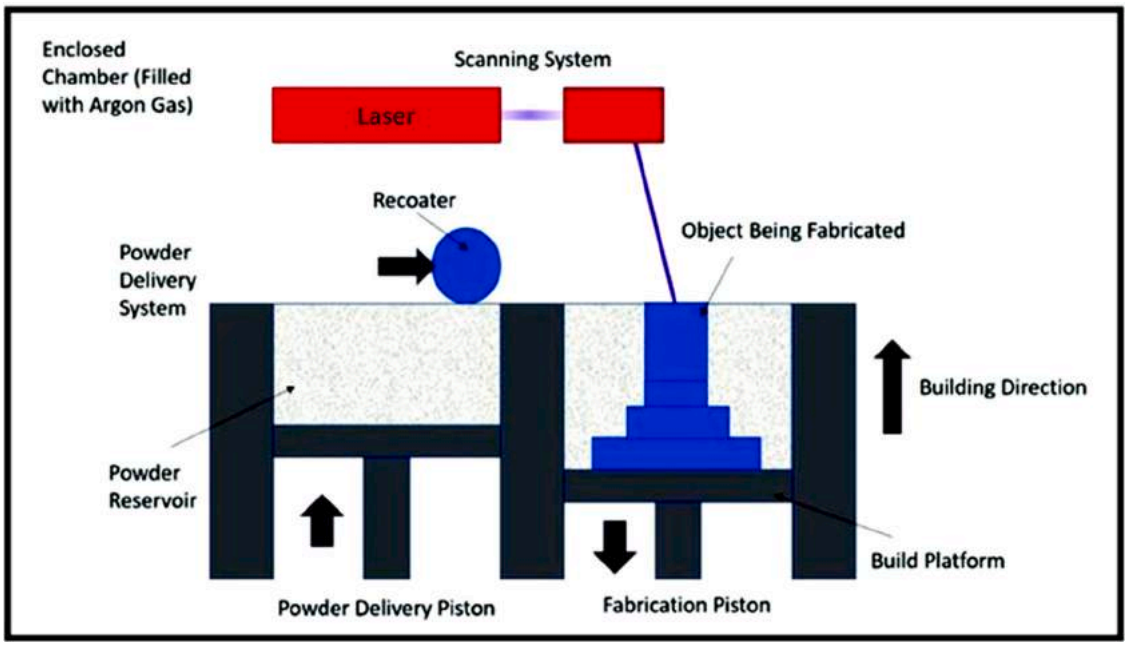

Fig. 2. Typical SLM process [209].

deployment device [35,36]. AM allows the creation of customized metal, ceramic and polymer components without the need for molds or tools. It is ideally established to become a significant pioneering element in the Fourth Industrial Revolution (IR4.0) [34,36].

Selective laser melting (SLM) is one of the AM methods that can produce bulk structural parts with almost no geometric limits. The word "selective" implies the processing of single or partial powder. The word "laser" signifies that a laser is used for processing, while the term "melting" indicates that the allocated powder is entirely melted [37]. This powder bed fusion method has the advantage of short production time and minimal processing steps [38]. Overall, SLM processing begins with designing the part to be manufactured using computer-aided design (CAD) software, based on a pre-tooled 3D model under a protective environment [16]. The SLM method involves a metallic powder that is being uniformly spread on the build platform and selectively melted by an energy source [39–41] consisting of a laser beam with an adjustable wavelength [18]. Fig. 2 shows a typical SLM technique.

SLM studies on (α + β) Ti materials had mostly considered the Ti-6Al-4V alloy to be commonly used for biomedical applications. Due to the high temperature of the SLM process, the microstructure of Ti-6Al-4V presents some fine (α + β)-type acicular martensite phases [42]. This distinctive microstructure leads to the better mechanical properties and ductility of SLM Ti-6Al-4V as compared to the conventional Ti-6Al-4V. Zhai *et al.* [43] claimed that it had the highest strength and reduced deformation. In addition, another (α + β)-type alloy (Ti–6Al–7 Nb) was previously studied as a replacement for the Ti-6Al-4V, which is commonly used in biomedical applications since the 1950 s [44]. Ti–6–7 Nb has higher corrosion resistance and shows some acicular martensite similar to SLM Ti-6Al-4V [45].

As shown in Table 2, the tensile characteristics of SLM Ti-6Al-4V give a maximum yield strength of 1110 MPa and ultimate tensile strength of 1267 MPa [46,47]. SLM Ti-6Al-4V samples were out performed due to their martensitic microstructure which might be regarded as a viable option for biomedical implants, as it can resist load-bearing in medical applications. Furthermore, the elastic moduli of the SLM (α + β)-type Ti–6Al–7 Nb were greater than those of the compact bone, which can be ascribed to residual stress and flaws when utilized as an implant [47,48]. Chlebus *et al.* [14] demonstrated that the SLM Ti–6Al–7 Nb showed high mechanical properties. However, the continuous cracks on the surface reduced the material ductility and post-treatment to improve the surface of SLM Ti–6Al–7 Nb was recommended. The yield strength and tensile strength of the SLM-type Cp-Ti are lower than those of the SLM Ti-6Al-4V, as shown in Table 2. This is due to the existence of fine acicular martensite pores caused by the cooling rate in the SLM process. In addition, Ti–24 Nb–4Zr–8Sn is a good example of a β-type alloy for biomedical applications as it has an elastic modulus of 49 GPa, which is closer to cortex bone of 20 GPa. The elastic modulus is lower than that of the conventional Ti-6Al-4V implants, and thus can reduce the stress-shielding effect [49,50]. However, due to the high O_2 level content of SLM processing material during the repeated melting process in SLM processing, the SLM-produced Ti–24 Nb–4Zr–8Sn displayed a significant reduction in ductility and strength [51,52]. These alloying elements are rare; hence, higher costs arise in obtaining and fabricating the raw materials. Ti-11 Nb-7Fe is another β-type alloy that presents an elastic modulus comparable to the human bone and excellent abrasive wear resistance compared to the α + β-type Ti alloys [53,54].

SLM is a complex process, and thus optimization of the processing parameters is needed to produce high-quality components. A study by Vilaro *et al.* [55] suggested that the uncontrolled pores in the SLM process for Ti-6Al-4V might deteriorate its material properties. They found that the pore orientation strongly influenced the macroscopic ductility of the Ti-6Al-4V. Biswas *et al.* [56] and Li *et al.* [57] revealed that the pores were likely to become microcracks that eventually reduced the SLM Ti-6Al-4V integrity in biomedical applications. Nevertheless, Kasporovich *et al.* [58] noticed that porosity of 0.08% remained under the optimized SLM parameters with pore sizes in the range of 50–300 μm. The pores occupied a substantial volume percentage of the SLM sample. Wysocki *et al.* [59] demonstrated that the surface treatment of SLM samples enhanced biomedical implant cell colonization and osteointegration properties. Bone regeneration and implant integration is also correlate to pore size, surface roughness, and elasticity of the SLM Ti-6Al-4V. Moderate elasticity and surface roughness (2–4 μm) reduce osteoclast activity and promote earlier healing. Elasticity, architectural similarity to cancellous bone and a pore dimension range between 450 μm and 650 μm are needed ensure interconnectivity as well as angiogenic and metabolic activity. AM-built parts are commonly

Table 2
Typical tensile properties of titanium alloys fabricated using SLM [60].

SLM processing Ti alloy	Tensile Strength [MPa]	$\sigma_{0.2}$ [MPa]	Tensile modulus E_t [GPa]	σ_{UTS} [MPa]	Strain failure [%]
Ti-6Al-4V	1070	1110	109	1267	7.28
CP-Ti	61	555	106	757	19.5
Ti–11 Nb–7Fe	1990	1144	86	985	32.1
Ti–24 Nb–4Zr–8Sn	50	563	49	665	13.8
Ti–6Al–7 Nb	1074	900	105 – 110	1000	12

subjected to post-processing in order to improve the pores for the attachment of cells.

SLM may also play a significant role in the medical and biomedical engineering industries since it can produce various instruments, prosthetics and implants, such as Ti bone models and acetabular cups [60]. As demonstrated, the high yield strength of Ti-6Al-4V improves the material's ability to resist deformation, which can benefit the patient in orthopedic applications. The moduli of Ti-6Al-4V alloys are still significantly higher than that of bone which may cause bone resorption and implant loosening [61,62]. Further decreases in Young's modulus of the Ti-6Al-4V material is still required not to exceed that of the human skeleton to reduce the impact of stress shielding, thereby supporting increased osseointegration [16,63,64].

3. Stress-shielding effect of SLM Ti-6Al-4V implants

The conventionally fabricated Ti-6Al-4V products had faced a common issue, including excessively high elastic modulus compared to human bone and the consequent stress-shielding effect. In general, stress shielding happens when the implant rigidity differs from that of bone. It increases tension at the bone-implant interface, which can cause the implant to fail. When this occurs, callus development is delayed, and the bone density is ultimately lost due to an implant inhibiting stress distribution of the bone [65]. Attempts have been made to reduce the tensile properties of Ti-6Al-4V parts fabricated by using the SLM technique. Table 3 summarizes several methods for reducing the stress-shielding effect that commonly occurs in Ti-6Al-4V implants. Many attempts were made to overcome this problem, including by controlling the porosity of the dense part [66–72], improving the pore dimensions [73,74], designing the implant as a lattice structure [27,75–81], structural build-up direction, heat treatment [82–87] and hot isostatic pressing (HIP) technique [88–91].

Porous structures which mimic the human bone structure are the future of orthopedic implantology. However, fully materials suffer from certain drawbacks. To overcome these, implants of different porosities can be prepared. Based on Eq. (1), porosity of an implant can be optimized to an appropriate value, and this attributes to a similar macrostructure to that of human bone, simultaneously improves tissue adhesion.

$$Porosity = \frac{\text{Pore Volume(Vp)}}{\text{Total Volume(Vt)}} \times 100\% \quad (1)$$

Additionally, surface characteristics, structural design, porosity, pore size, shape and orientation play an essential role in bone growth on biomaterials. Chen *et al.* [66] fabricated Ti-6Al-4V with approximately 40–80% porosity. It can be claimed that as the porosity of the sample increased, compressive modulus was significantly decreased. To obtain a comparable result to human bone, an optimal porosity value of 67% for a Ti-6Al-4V implant was recommended. Gibson and Ashby's model was used to estimate the modulus and yield of SLM Ti-6Al-4V and it was found that the structure with a modulus of 15 GPa and yield stress of 129 MPa corresponded to the strength of human bone. To meet this criterion, Soro et al. [68] created porous SLM Ti-6Al-4V via a solid network built on a Schwartz primitive unit-cell. The 25% and 42% porous samples broke into two pieces during loading, whereas the 64% porous sample was intact. The 25% porous sample was found to have a fracture surface as compared to the 64% sample. Mechanical testing findings for the 64% porous samples matched the cortical bone characteristics, with stiffness of 22.3 GPa and yield strength of 160 MPa. A study by Xu *et al.* [68] reported that the compressive modulus and strength of the porous structure decreased with increase in porosity. The modulus of porous structures with porosity of 60% and cell size close to 1 mm was comparable to trabecular and cortical bone. Arjunan *et al.* [70] studied similar porosities which ranged from 60% to 90% and showed that the pore shape influenced permeability and strength of the SLM sample. The porosity of 60% gave an effective modulus of 10.42 GPa and compressive strength of 152.30 MPa. However, the modulus value was twice that of the anatomical bone. The honeycomb-shaped pores at 74.31% porosity showed a good balance of higher surface fraction for oxygen transport into the scaffold and exhibited 0.91 GPa compressive moduli. Falkowska *et al.* [71] used SLM to fabricate a novel diamond structure shape with varying porosity, and a compressive modulus value of 3.7 GPa at 81% porosity was reported. This value was close to corresponding with that of human bone. However, at 73% porosity, the study found different sizes of beads on the sample surface, which indicated the "balling effect" common in SLM processing, as illustrated in Fig. 3. The size of the balls was observed with diameters of up to 100 µm. The authors recommended post-processing to improve the surface texture. Studies by Li *et al.* [92] demonstrated that the 75% porosity sample showed a compressive modulus of 1.76 GPa and the characteristics were similar to the trabeculae. Moreover, it was able to provide support without significant stress shielding. On the other hand, the 50% sample had a compressive modulus almost twice the 75% porosity sample value. The osteogenic differentiation and alkaline phosphatase (ALP) activities on the 75% sample were higher than those of the denser 50% sample. This was due to the high porosity samples which provided a sufficient space for the human bone to grow and at the same time facilitated an adequate supply of nutrients. As for 55% porosity, Stepanov *et al.* [93] found that the SLM Ti-6Al-4V surface showed uniform intragranular structures due to the dissolution of the α phase after heat treatment at 780°C for 1 h under high pressure. The removal of the quenching stresses and decomposition of α-martensite showed an increase in plastic deformation of up to 50% on the 55% porosity sample. This caused a substantial increase in compressive strength to 130 MPa, which increased 30% from the untreated sample. Sample that was treated at 780 C showed an elasticity modulus of comparable value with compact human bone. However, as the annealing temperature was increased to 920°C, the tensile decreased to 90 MPa, respectively.

Wu *et al.* [72] determined the fatigue failure of SLM Ti-6Al-4V with different porosities and reported that increasing the porosity improved the fatigue endurance performance, making them advantageous for long-term application in biomedical applications implants. This improvement attributed to the phase transformation of brittle α'-martensite in the SLM processing, as illustrated in Fig. 4 (a). The increase in the mechanical properties correlates to the acicular α/α′ martensite within β lamellar of the SLM Ti-6Al-4V. As in Fig. 4 (b) HIP treatment has changed the microstructure from the

Table 3
Typical methods for improving the mechanical properties of the SLM Ti-6Al-4V from earlier work.

Ref.	Year	Method	Parametric study	Compressive strength (MPa)	Compressive modulus (GPa)	Remark
Pei *et al.*[100]	2017	Lattice Structure	Strut diameters were set to 200, 250, 300, 350, and 400 μm	60	3.15	The porosity of the SLM sample decreased with the increase in strut diameter/
L.Y. Chen *et al.*[106]	2017	Build Direction	X, Y and Z Plane	–	4.20	Exhibit no significant difference in modulus.
S.Y. Chen *et al.*[66]	2017	Porosity	40%, 50%, 60%, 70%, and 80%	62.00	9.70	Compressive modulus decreases when porosity increased.
Didier *et al.*[75]	2017	Lattice Structure	The anatomical and standard model	–		The anatomical model showed stress on the bone when tightening with compression screws.
Xu *et al.*[68]	2017	Porosity	20%, 30%, 40%, 50%, 60% and 80%	48.00	4.02	With increasing porosity, the elastic modulus and compressive strength of porous structures decrease.
Bartolomeu *et al.*[73]	2017	Pore size	100 μm, 200 μm, 300 μm, 400 μm, and 500 μm	–	–	100 μm showed reduced modulus but 500 μm showed higher stress on the sample.
Zaharin *et al.*[101]	2018	Lattice Structure	Cube and gyroid	22.40	3.69	The strut of a 0.3 mm gyroid showed promising mechanical properties similar to anatomical bone.
Bai *et al.*[76]	2018	Lattice structure	AFCC and BCC	42.87	0.78	AFCC showed improvement in compressive modulus.
Kadirgama *et al.*[77]	2018	Lattice Structure	Honeycomb	–	0.22	Built structures have a compressive modulus ranging between 0.01 and 1.84 GPa.
Stepanov *et al.*[93]	2018	Porosity	55%	73		The strength of the SLM Ti-6Al-4V increased up to 30%.
Zhang *et al.*[78]	2018	Lattice Structure	Bone design	27.1	3.7	Modulus decrease when porosity increased.
Cho *et al.*[107]	2019	Build direction	Bottom to top in the z plane	–	–	Modulus of the top surface was the lowest.
Peng *et al.*[79]	2019	Lattice Structure	LSRCMS	21.36	2.23	Compressive modulus decreased when porosity increased.
Li *et al.*[104]	2019	Lattice structure	Trabecular Cup	98.55	1.96	HA coated sample showed a significantly higher value of elastic modulus (106.33 GPa) far from that of anatomical bone.
Elsayed *et al.*[108]	2019	Build Direction	Vertical of Z plane	–	–	Porosity decreased with decreasing scan speed and hatching spacing, resulting in complete melting of the powder on the surface.
Lan Li *et al.*[103]	2019	Lattice Structure	TPMS	43.57	3.073	The push-out force reached up to 110–1300 N 5 weeks after implantation.
Soro *et al.*[69]	2019	Porosity	0%, 25%, 42% and 64%	53	1.6	400 μm samples match the properties of cortical bone.
Wally *et al.*[27]	2019	Lattice structure	Spider web	16	0.7	The sample's compression stiffness was within the normal range for cancellous bone.
Arjunan *et al.*[70]	2020	Porosity	68.46%, 70.25%,74.05%, 80.17%, 81.14%, and 90.69%,	39.49	2.21	Pore shape influences permeability, stiffness, strength and the stress concentration.
Falkowska *et al.*[71]	2020	Porosity	34%, 50%, 73% and 81%	50.3	3.7	Fracture on the surface at 34% porosity.
Cheong *et al.*[105]	2020	Lattice structure	Intramedullary Nail	–	0.5	Mature bone formed on the 700 μm pore lattice.
Ge *et al.*[80]	2020	Lattice structure	Trab and TPMS	34.62	5.51	Trab and TPMS lattices were comparable to bones.
Wu *et al.*[72]	2021	Porosity	33%, 50%, and 84%	47		When the stress cycle fell below 70%, fatigue strain accumulated.
Bartolomeu *et al.*[81]	2021	Lattice structure	Cellular structure mimic cells	–	–	Inefficient and non-uniform stress distribution on surface of implant.
Meng *et al.*[74]	2021	Pore size	100 μm, 300 μm, 500 μm, and 1000 μm	–	–	The unmelted powders accumulated on 1000 μm pores.
Pereira *et al.*[95]	2021	Pore Size	400 μm	–	3.76	Higher DNA content was observed in SaOS2 cells.

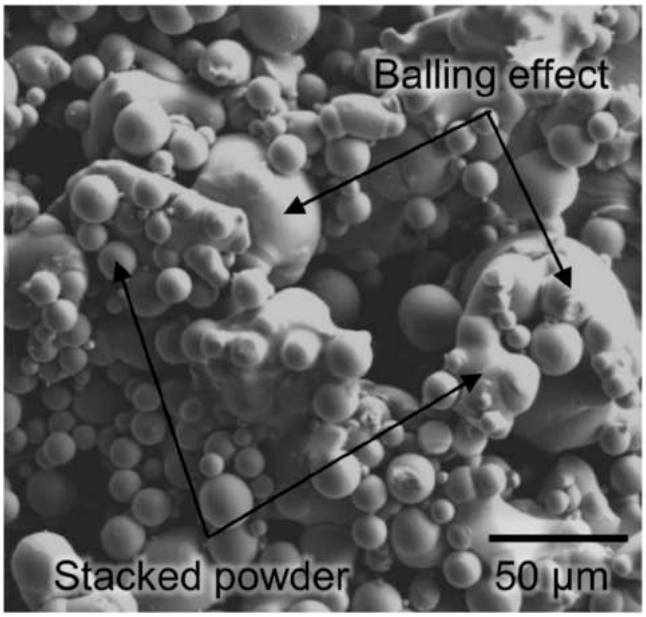

Fig. 3. Balling effect on the surface of SLM Ti-6Al-4V [210].

α'-martensitic structure into α' + and at the same time improved the fatigue endurance. The HIP process demonstrated coarsening of the microstructure, due to the presence of coarse α and β between the lamellar.

The production of cellular/porous structures by additive manufacturing technologies like SLM offers several advantages, such as total control of pore size, orientation and homogeneous pore distribution, which resulted from a pre-designed pattern. To this end, several studies investigated the pore size on the surface of implant, aiming at increasing bone ingrowth and bone-bonding strength. Meng *et al.* [74] studied the influences of embedded pore location and discovered that it did not affect compressive modulus or strength. However, the study showed a significant finding on fracture elongation. It was discovered that a pore size of 1000 μm produced the best elongation to failure, which was between 6% and 12%, and thus was very close to bone fracture strain. Nevertheless, there was a massive layer of unmelted particles on the outer surface in the shape of caviar, which was noted as being favorable for cell ingrowth. Taniguchi *et al.* [94] suggested that larger pore sizes (> = 900 μm) might lower the bone ingrowth ratio, which might be related to the drop in the efficiency of local bone replacement and biomechanical activation from the substrate. However, a pore size of less than 400 μm might restrict cell access and the transmission of nutrients or oxygen to the implant site, resulting in insufficient vascularization and also bone resorption. The previous study also noted that a pore size between 400 μm and 600 μm was recommended to enhance blood capillaries in bone formation[37]. Bartolomeu *et al.* [73] developed a Ti-6Al-4V implant with various open-pore structures and discovered that a pore with a length of 100 μm had a substantial effect on the modulus and strength. The study found that by changing the microstructure of the titanium alloy, mechanical properties were comparable to those of cortical bone. Moreover, this void dimension can also enhance the friction and wear performance of the implant. In contrast, the weight loss was greater in a sample with a pore size of 500 μm, and cracks were more easily formed in areas of high-stress concentration caused by these massive voids. Pereira *et al.* [95] produced SLM Ti-6Al-4V with an open pore size of 400 μm and obtained surface roughnessRa = 0.966 μm. The experimental results showed Ti-6Al-4V scaffolds exhibited a modulus of 76.85 GPa, which was relevant in bone tissue engineering solutions to reduce the stress-shielding phenomenon. After 14 days of *in vitro* cell culture in SaOS-2 cells, higher DNA content was observed. Anyway, comparing Day 3 and Day 7 the ALP activity was reduced. This indicated that the peak of expression was highest during the first seven days, whereby the osteogenic cells stimulated bone remodeling, a continuous increase in the proliferation rate and insufficient cell-cell contact (Tang *et al.*)[96].

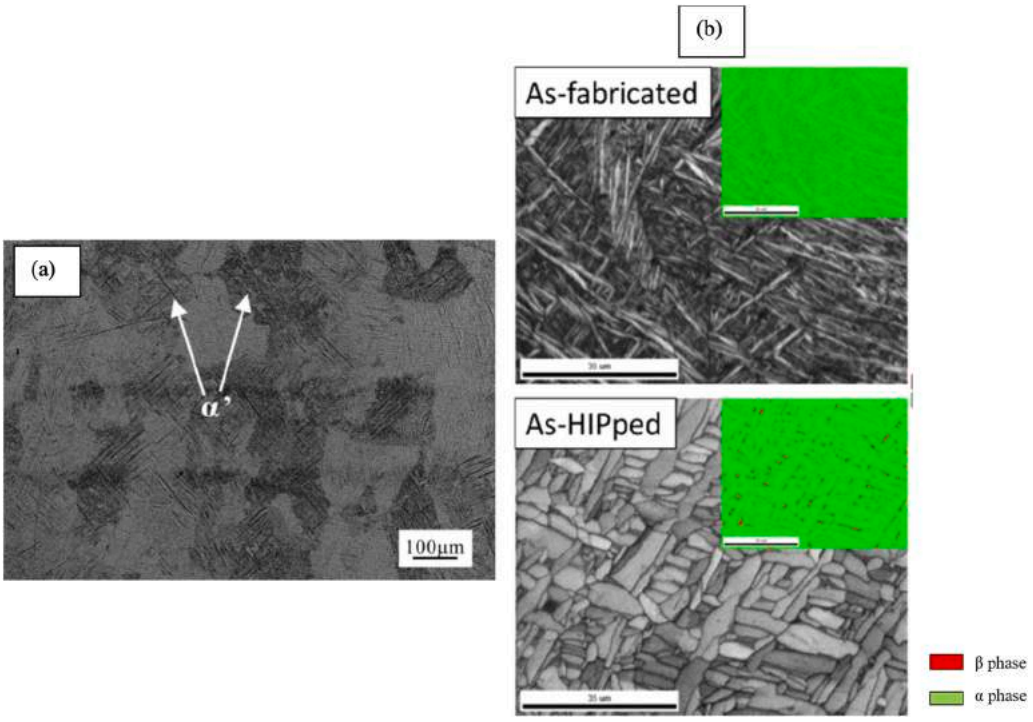

Fig. 4. (a) Micrographs of α martensite on SLM Ti-6Al-4V [211], (b) as-build and post-HIP Ti6Al4V [28].

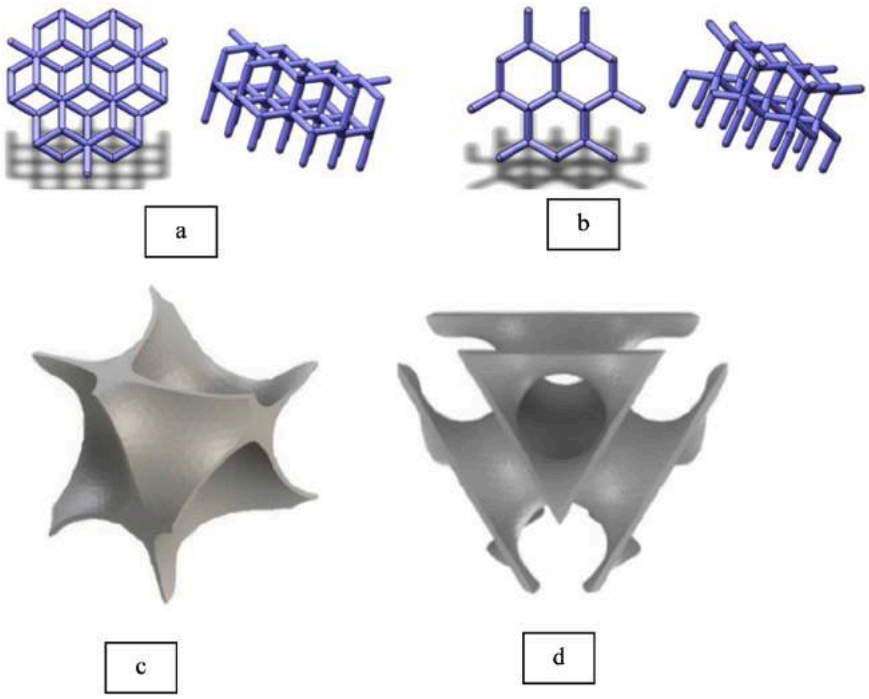

Fig. 5. The structural unit of (a) DFCC[212] (b) DHEX[212] (c) gyroid TPMS[213] and (d) Schwartz diamond FGS[213].

A lattice structure is made up of a series of spatial arrangements of unit cells that have edges and faces. These cellular solids can be found in two or three dimensions [97]. Lattice structures can commonly provide solutions in a variety of disciplines, including the medical, aeronautical and automobile industries, since they offer advantages such as reduced weight, increased energy absorption and reductions in cost and production time. A lattice structure can improve mechanical performance in ways linked to its porosity and relative density. Fig. 5, shows the common lattice structures of AM implants. The diamond lattice structure (DFCC) (Fig. (5a)) and hexagonal diamond lattice structure (DHEX) (Fig. (5b)) have the same crystal and structural unit. On the other hand, the gyroid TPMS illustrated in Fig. 5(c) has morphological features with a bone-mimicking architecture and possesses superior strength (152.6 MPa) and comparable elastic modulus (3.8 GPa) with natural cortical bone [98]. As shown in Fig. 5(d), the functionally graded porous (FGP) scaffold based on Schwartz diamond has become an attractive option for a bone graft candidate due to its improved mechanical and biological requirements that included surface area with porosities of 60% and 80%, as reported by Maszybrocka *et al.* [99].

Bai *et al.* [76] proposed a lattice structure to reduce weight and enhance the mechanical properties of a structure. The result demonstrated that the all-face-centered cubic (FCC) design (Fig. 6(b)) was superior to a body-centered cubic (BCC) (Fig. 6(a)) structure, whereby the tensile modulus and yield strength increased up to 143% and 120%, respectively. The tensile modulus values for FCC and BCC were 787.1 MPa and 1917 MPa, increasing the modulus caused by the stretching process. As for biomedical implants, the modulus is far beyond that of cortical bone, resulting in a stress-shielding effect.

Wally *et al.* [27] showed that the spider web pore shape yielded a similar compressive modulus and strength to the dense sample. There were higher mechanical properties in samples with a dense core and thicker struts. The scaffolds exhibited the highest modulus and yield strengths with a 'spider web' structure and 2 mm dense core, while the weakest scaffolds had 650 µm pores. Compressive modulus and strength were lower with increasing porosity, as expected from a previous study in which Peng *et al.* [79]. This study evaluated SLM Ti-6Al-4V with various pore sizes in a hexagonal shape and predicted the compressive modulus and strength of the sample by using the Gibson-Ashby model. A circular structure gave lower modulus and compressive strength as compared to the rectangular form. The study correlates with other studies which claimed that the modulus decreased with increasing porosity in the uniaxial compression test. A study by Ge *et al.* [80] demonstrated the trabecular lattice structure (Trab) and gyroid triply periodic minimal (TPMS) had a significant effect on the microstructure of SLM lattice. The Trab structure indicated a higher compressive strength and elastic modulus of 5.58 GPa than the TPMS (5.51 GPa). Both results showed a desirable compression modulus comparable to the compact bone (0.022–21 GPa). Kadirgama *et al.* [77] demonstrated that

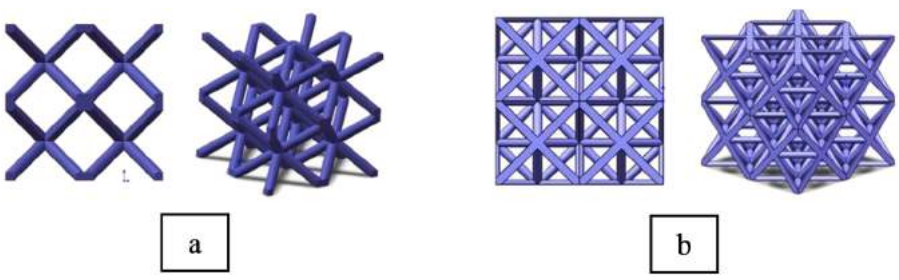

Fig. 6. Selective laser melting (SLM) forming sample of (a) BCC (b) AFCC [212].

lattice structures with different struct sizes showed various values of compressive modulus. The Ra value for lattice structures ranged from 8 µm to 13 µm at the top and side of sample, respectively. They exhibited a lower modulus value of 0.4 GPa which was close to that of femoral trabecular bone when the porosity was at 90%. [73]. The study concluded that the small irregular pores on the SLM Ti-6Al-4V contributed to the high residual stress, leading to a higher compressive modulus. Zhang *et al.* [78] revealed that the compressive modulus (3.7–5.7 GPa) and strength (27.1–84.7 MPa) of the SLM Ti-6Al-4V were obtained when it was built as a functionally graded scaffold with a design based on bone architecture. The scaffold design with varying strut sizes and densest porosity was discovered to be at 75% porosity. However, after heat treatment at 900 °C for 2 h and cooling inside a tube furnace, the sample yield strength was reduced by up to 56%, owing to substantial changes in the structural porosity that made the sample fracture easily. Pei *et al.* [100] fabricated SLM Ti-6Al-4V with lattice structures with various struct diameters from 200 µm to 400 µm. The pore was fixed at 630 ± 50 µm by adjusting the structs range and a force of 300 N was exerted to stimulate the compressive mechanical strength. The result demonstrated that porosity of the SLM sample decreased with an increase in strut diameter and the sample showed Ra < 10 µm, which can promote cell adhesion. A strut diameter of 0.3 mm showed a compressive strength of 31.5 MPa while the 0.35 mm strut sample showed 76.8 MPa, slightly lower than that of cortical bone (80 MPa) but higher than for spongy bone (20–40 MPa). On the other hand, the compressive modulus values obtained were approximately 3.61 GPa, lower than the comparable bone but slightly higher than the spongy bone. An *in vivo* animal model demonstrated that the implant remained intact, indicating successful osseointegration. Zaharin *et al.* [101] fabricated cube and gyroid lattice structures with various strut diameters, whereby the gyroid showed a porosity of 70–80% (within the value for natural bone). Forces of between 250 N and 4 kN were applied and the result showed a linear decrease of compressive modulus with the growth of porosity along with the pore size. For the 0.3 mm strut gyroid, the modulus of 10.6 GPa was within the range of compact bone while for the largest strut (0.6 mm), the value obtained was 5.6 GPa, similar to cancellous bone. The strength of bone was between 20 MPa and 190 MPa [102] and the study demonstrated a compression strength of 22.44 MPa, within the range of bone. The study found that a strut of 0.3 mm diameter in a gyroid design showed promising mechanical properties similar to anatomical bone. Li *et al.* [103] designed a scaffold based on TPMS modeling to mimic the human bone and porosity of 49.54% exhibited the lowest compressive modulus of 3.07 GPa, comparable to that of cancellous bone, with a compressive strength of 353.4 MPa. After implantation in the tibial bone of a Bama pig, the study found that bone formation was weak between the implant, but for the biomechanical test, the push-out force reached up to 110–1300 N at five weeks after implantation.

Since additive manufacturing (AM) is presently gaining traction in the medical industry, a custom-made implant should be based on the anatomical structure of human bone. Didier *et al.* [75] implanted a compression screw on SLM fabricated Ti-6Al-4V. The study involved two types of models based on the standard and anatomical models which were fabricated by using SLM Ti-6Al-4V. The anatomical model sample was adapted to the patient's morphology and reduced the stress field when implanted. However, the study found that after tightening the screw, the implant morphology stressed the bone and led to the stress-shielding effect. Bartolomeu *et al.* [81] fabricated SLM Ti-6Al-4V with different sub-millimeter cellular structures with various open-cell and wall sizes. The 600 µm cellular structures with a wall size of 100 µm exhibited an elastic modulus of 12.4Gpa, which matched the bone and demonstrated that the sample could be used in orthopedic applications. This was caused by the partially melted powder in the laser-melted zones increasing the thickness of the walls, consequently decreasing the open-cell dimensions. Li *et al.* [104] fabricated an uncoated and HA-coated lattice structure similar to the acetabular cup for implantation at the hip joint. The study found that the porosity of uncoated cup was 76.08% and the pore size was 508.57 µm. Average elastic modulus of the uncoated cup was 1.96 GPa, which matched that of cancellous bone, and a compressive strength of 98.55 MPa, which was comparable to compact bone. However, the HA-coated lattice showed a significantly higher modulus value (106.33 GPa), which was very different from that of the anatomical bone, making it unsuitable for acetabular cup implantation. After 1 year of *in vivo* beagle implantations, there was twice the degree of bone-implant contact (BIC) with uncoated bone as compared to the HA-coated group. This was due to the uncoated porous implant with higher porosity and large pore size, allowing more body fluids to be transported through the interconnected pores, which accelerated the healing process. As for complex femoral shaft fracture, intramedullary nails are commonly used by being inserted into the medullary cavity of the bone to provide solid support for the fractured bone. Cheong *et al.* [105] utilized SLM Ti-6Al-4V by fabricating intramedullary nails for long term implant applications. The nails were fabricated with 700 µm and 1500 µm pores. The compressive modulus obtained was 0.5 GPa, closely similar to trabecular bone. After six weeks of implantation in the long femur and femoral condyle, mature bone formation indicated direct reaction from the open reduction internal fracture (ORIF) surgery. For the 700 µm model, hard callus formed around the implant, as shown in Fig. 7, indicating successful bone remodeling. There was also a 23% reduction in stress concentration from 534 MPa to 411 MPa as compared to 1500 µm pore nails which provided 21% reduction.

Some studies focused on the build direction of the SLM process in the fabrication of Ti-6Al-4V to alter the modulus for biomedical application [106,107]. In the SLM process, the laser scan is moved back and forth in the Z-plane (perpendicular to the X and Y planes), and the product is built cumulatively from the bottom to the top along this plane shown in Fig. 8.

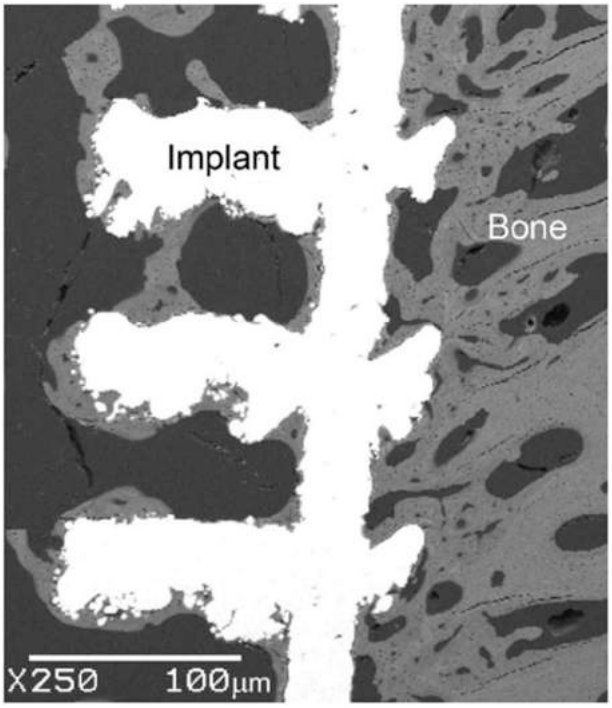

Fig. 7. (SEM) of the bone-implant interface for 70% porosity implant 6 weeks after implantation [105].

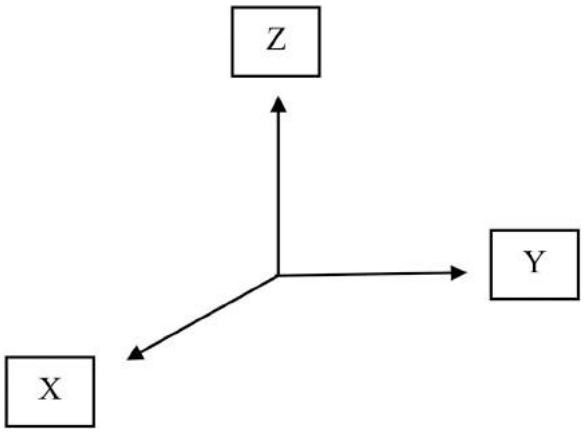

Fig. 8. The schematic diagram of SLM processed samples with the X-, Y- and Z-planes.

Cho *et al.* [107] demonstrated that the elastic modulus decreased linearly when the direction of the build was in the z-direction from mid-height to top. Nevertheless, the elastic modulus of the top surface was the lowest caused by the α′-martensite transformation back into the β form due to the increased temperature to above the β-transus in the build direction of the SLM Ti-6Al-4V. α′-martensitic Ti-6Al-4V could be beneficial in yielding strength in implant applications. Nonetheless, Chen *et al.* [97] proved that the modulus of SLM Ti-6Al-4V was equivalent to 127 GPa and that there was no significant variation in any plane. From this study, the SLM processed samples maintained the original composition and crystal of powder structure. The modulus for all three planes was closely similar, attributable to the similar atomic bonding of Ti-6Al-4V atoms in each X, Y, and Z plane. In this study, it was found that the X-plane exhibited the worst response as compared with the Y-plane and Z-plane with the hardness of the X-plane being lowered by 20%. After immersion in SBF, defects were found on the implant surface attributed to the chemical corrosion contact in Hank's SBF of the SLM samples. Elsayed *et al.* [108] built SLM Ti-6Al-4V using a vertical Z-increment of 30 µm under an Argon atmosphere and measurements were made for each sample - two at the bottom followed by the bottom two at the top. The study showed that the porosity decreased with the decreasing scan speed and hatching spacing, resulting in complete melting of the powder on the surface. The modulus obtained was 30 GPa, corresponding to the cortical bone with a compressive strength of 522 MPa when the scan speed was 400 mm/s followed by 99 µm hatch spacing.

In summary, the previous study showed that to reduce the stress shielding of SLM Ti-6Al-4V, various methods were used to decrease the high value of the compressive modulus and strength of SLM Ti-6Al-4V. For the pore structure, it was shown that a pore size between 400 µm and 600 µm exhibited better reductions in the modulus while at the same time improving the cell remodeling at the fracture sites and surface of the implant. On the other hand, it was found that porosity in the range 60–70% should improve bone remodeling and reduce the modulus to levels comparable to compact bone. Porosity, pore size and mechanical properties can be easily modulated by adjusting the pore-unit parameters to achieve the bionic design of bone tissue implants. The higher porosity of porous materials with larger pores can allow the bone to grow into the increased pore spaces. On the other hand, the lattice structure, is

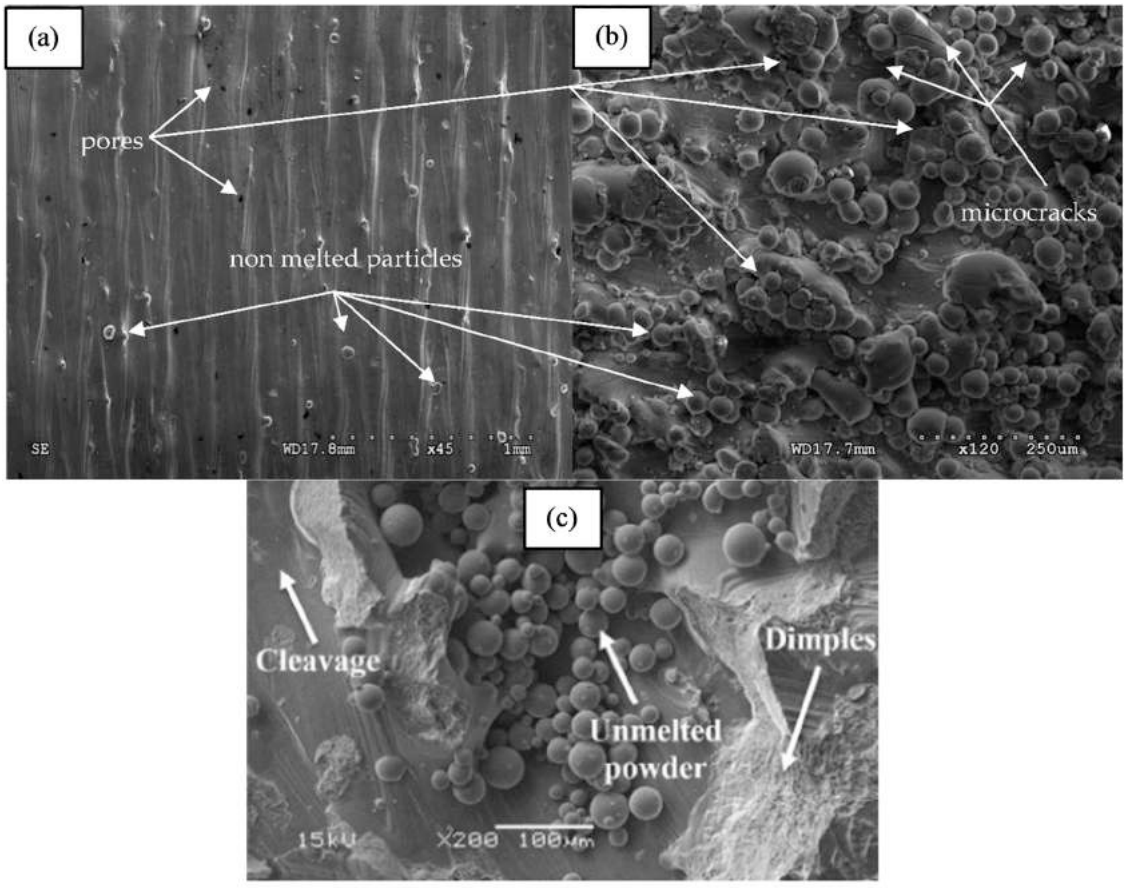

Fig. 9. Typical surface morphologies of Ti-6Al-4V fabricated using SLM at a (a) power (*P*) = 120 W, speed (v) = 0.2 m/s[214] (b) power (*P*) = 110 W, speed (v) = 0.4 m/s, [214] and (c) power (*P*) = 110 W, speed (v) = 1.2 m/s[215].

able to mimic the bone while at the same time improve the cell attachment. Therefore, a balance between the microstructure and the mechanical properties is very important for better porous implant performance. It can be seen that some of the fabricated SLM implants showed some unfavorable impurities and oxide layers on the surface of implant. Further, post-processing is needed to improve the surface of implant. The implant surface roughness also plays an important role for a biomedical implant as it affects the attachment of cells and osseointegration.

4. Surface treatment of Ti-6Al-4V biomedical implant

The SLM samples generally offer a better surface quality than EBM as the powders are held at a much higher temperature during EBM, along with higher energy input and larger spot size [109]. Compared to SLM, heat dispersion out of the melting pool in the powder bed is more likely, resulting in a much inferior surface finish [110,111]. However, uncontrolled SLM parameters could degrade the microstructure and orientation of the Ti-6Al-4V surface [112]. The energy density (E) is a significant factor that influences the components produced. It is measured as follows:

$$E = \frac{P}{vht} \tag{2}$$

Where, P = laser power, v = scan speed, h = pitch and t = thickness of the layer [113]. According to Eq. 2, increasing the laser power enhances energy density and, as a result, it increases the chance of a molten metal being produced [114,115]. The amount of laser energy delivered must be adequate to melt, solidify, and generate ideally dense structures with increased durability when in contact with living cells [64,113].

Fig. 9 depicts typical surface morphologies of Ti-6Al-4V produced by SLM at various laser power (P) and scanning speed settings (v) [116]. As shown in Fig. 9(a), at a power of 120 W and a speed of 0.2 m/s, a relatively dense surface component is formed. Nevertheless, this tend to produce a split surface with numerous cracks, flaws that are harmful to the efficiency of osseointegration permitted by the SLM product. Fig. 9(b) portrays the reasonably smooth melted surface when the SLM is operated at 110 W and the laser is run at 0.4 m/s. Also, it may be seen that unmelted particles exist, and these can be identified as the balling phenomenon which can be explained by the melting instability that occurs during the selective laser melting process. However, raising the scanning speed to 1.2 m/s increases the amount of balling and creates a porous titanium unit cell with a helical pore structure [113,117] and a sintering neck feature (Fig. 9(c)). This was due to inadequate energy input and the diameters of the unmelted particles were significantly enlarged [64,113,116]. Inadequate melting temperature results in porous structure with low-quality and low mechanical strength that unsuitable to be used for biomedical implants.

Furthermore, porous implants with a rough surface may stimulate osteoblastic proliferation and integration along with the implant-tissue interfaces [117–119]. Fig. 10 represents the relation between laser scanning speed and surface roughness on the side and top view for a Ti-6Al-4V alloy manufactured using the SLM method. Fig. 10(a) indicates that raising the scanning speed to 775 mm/s resulted in an increase in surface roughness of 0.65 µm on the side of the sample. However, the Ra value of 4.49 µm was reached on the top surface, as shown in Fig. 10(b). Significantly, the top and the side parts fabricated by using a low scanning speed of 697.5 mm/s showed a low roughness value.

In general, the surface roughness of the SLM (Ra: 5–40 µm) product is smoother than that of EBM (Ra: 25 µm – 130 µm) processes, which promotes cell adherence when used as an implant [120]. Ginestra *et al.* [121] examined cell attachment on different surface topologies of the Ti-6Al-4V implant created by SLM and EBM. It was discovered that SLM samples can substantially increase pre-osteoclast cell proliferation and speed mineralization than EBM samples. Osteoblasts prefer rough surfaces with Ra values of 3–5 µm for attachment *in vivo* and *in vitro*. Materials with roughness levels above this range did not necessarily promote osteointegration in the prior investigation [11]. However, it was proposed that implant roughness ranges between 1 µm and 2 µm range is effective for developing a titanium dioxide (TiO_2) layer that is resistant to bacterial infection [119,122,123]. As a result of this, surface treatment of the Ti-6Al-4V produced by using the SLM process must be encouraged to enhance cell adhesion.

Table 4 summarizes investigations on implant performance after surface treatment of a Ti alloy produced by using the SLM method. Surface treatment of implants is a subtractive technique of altering the surface roughness, modifying the implant topography, and improving the biological response before implantation. This eventually can enhance bone regeneration and biomechanical stability. There are three categories of treatment, namely acid treatment, acid etching and an alkali-acid treatment combination. In general, acid treatment refers to the surface treatment of Ti-6Al-4V with a mixture of sulfuric acid (H_2SO_4) and hydrochloric acid (HCl). For example, Wild *et al.* [124] evaluated the osteoconductive properties of Ti-6Al-4V fabricated using SLM. The samples were first blasted with corundum particles and then treated in a hot acid mixture containing 32% HCl and 95% H_2SO_4. The number of cells adhered to the treated implant was roughly 1.31 times higher than the untreated Ti samples, indicating that the sample may be used therapeutically for reasons of bone augmentation. According to Xu *et al.* [125], the existence of micropores via surface treatment of SLM titanium considerably increased osteoblast proliferation, protein content, bone-implant contact (BIC) behavior and bone-bonding interaction. It was found that the mixture of 98% H_2SO_4 and 36.5% HCl solution yielded the highest surface roughness of 7.63 µm due to eliminating the particles' irregularities. However, this concentration opposes the observations of Wild *et al.* [124] in which the bone-implant contact percentage of modified Ti alloy was nearly double that of the native sample.

Furthermore, acid etching has a positive influence on bone remodeling by the presence of hydrofluoric acid (HF) within the sulfuric acid(H_2SO_4) nitric acid (HNO_3) and hydrochloric acid (HCL) acid mixture that used to study metallic alloy and Ti-6Al-4V. Van Bael *et al.* [126] stated that the Ti-6Al-4V manufactured by SLM with a pore size of 1000 µm obtained a significant increase in cell attachment compared to an implant pore size of 500 µm after treatment with 48% HF. The study found that the pore shape did not influence the growth of the cells. However, pore size played a significant role in cell attachment. Also, Wysocki *et al.* [127] constructed a porous implant with pore sizes of 200 µm, 500 µm and 200 + 500 µm. It was then polished the sample with HF and HF+HNO_3 acid solutions between 1 min and 9 min. This study mentioned that the mixture of HF +HNO_3 solution successfully produced the SLM sample with a pore size as small as 200 µm and a decrease in the water contact angle of between 52% and 75%. The inclusion of HF increased the production of soluble compounds and reduced hydrogen embrittlement, whereas the addition of HNO_3 improved titanium passivation. The samples of Ti-6Al-4V became brittle and prone to fracture as a reduction of hydrogen embrittlement, which decreased the interaction between the implant and attachment of mesenchymal stem cells. Wang *et al.* [128] fabricated SLM Ti-6Al-4V with closely spaced and irregular lattice structures. Then, the samples were treated with a combination of sandblasting and acid etching. It was observed that the treated SLM samples produced many micro pits and micro-cavities with sharp edges on the surface. Compared to the untreated samples, the SLM samples resulted in an increased Ra value nearly 2.92 µm. Meanwhile, *in vivo* experiments indicated a more osteophilic environment that aided the growth of human bone marrow

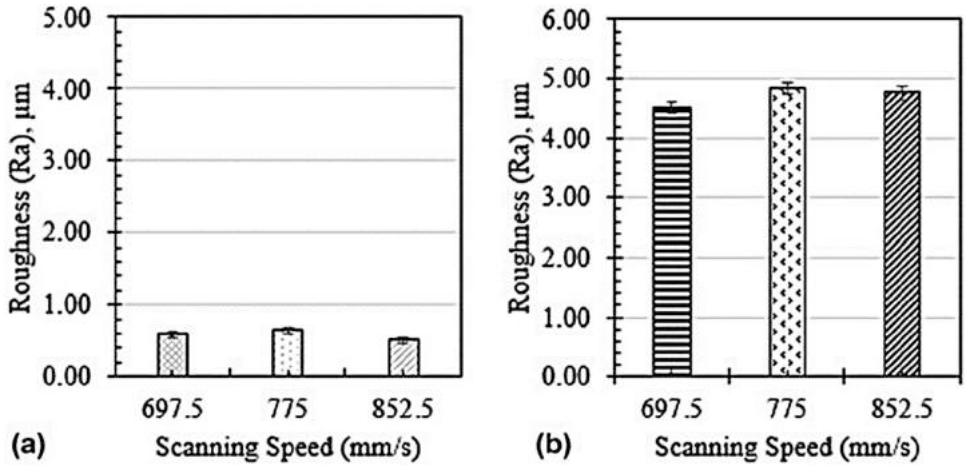

Fig. 10. Influence of SLM scanning speed on the roughness (a) on the side and (b) on the top of a Ti-6Al-4V sample [216].

mesenchymal stem cells (hBMSCs) and increased osteo-related mRNA levels in the samples. Nevertheless, Balykin *et al.* [129] and Thenard *et al.* [130] used a combination of HF and 10%HNO_3 to treat the SLM Ti-6Al-4V. Several defects appeared after the etching process caused by the residual stress, which reduced the surface roughness and increased wettability. This could hinder the adhesion of cells in biomedical applications as higher wettability may reduce cells attachment on the surface of implant and the high concentration of HNO3 alters the oxide layer of the SLM sample, leading to defects. The work by Jamshidi *et al.* [28] and Vayssette *et al.* [131] also suggested that the combination of HF and HNO_3 could improve the surface topology of the SLM samples. The chemical etching with 1–2% HF significantly reduced surface roughness, eliminating crevices and imperfections. This method reduced the crack formation and improved the cellular affinity of the growth cells on the surface of the SLM samples. Most importantly, the study noticed that the surface of SLM Ti-6Al-4V showed higher cellular affinity and metabolic activity of growth cells for tissue integration on the implantation site after 14 days *in vitro* cell culture. This research revealed that chemical etching had a significant impact on the cellular affinity of the SLM substrate. For example, Fig. 11 illustrates typical SEM images for Ti-6Al-4V produced by using SLM. The untreated Ti-6Al-4V exhibited many fracture initiations due to poor surface roughness, as shown in Fig. 11(a), impacting the cell biological response and adhesion [28]. However, when a sample was treated with a combination of HF and HNO_3 the crevices and irregular imperfections on the surface were eliminated. The decreasing the crack formation increased the metabolic activity of seeded cells on the surfaces (Fig. 11(b)) [132,133].

Gonzales *et al.* [134] described the roughness of the acid-etched surfaces treated with 50% H2SO4 and 50% HCl were slightly lowered than the as build SLM. Nonetheless, the study mentioned that a treated surface had more micropores which enhanced the alkaline phosphatase (ALP) bioactivity of implant to spread osteoblast and osteoclast cells. Le *et al.* [135] proved that the SLM Ti-6Al-4V sample treated with a combination of H_2SO_4 and HCl increased the surface roughness. This stimulated the osteoconductivity of the implant in MC3T3-E1 cells and increased the apatite formation in simulated body fluid (SBF). The study found that the cell viability was largely improved after 3-day exposure for the post-chemical heat treatment. However, there were no substantial improvements in ALP activity between heat-treated and non-heat-treated samples.

In addition, some studies focused on the combination of alkali-acid treatment, whereby sodium hydroxide (NaOH) was used in combination with HCl to improve the surface roughness of titanium alloy. To evaluate the implant osteoblast induction, Fukuda *et al.* [136] used an SLM-built Ti-6Al-4V structure with varying surface porosity and immersed it in a mixture of 20% NaOH and 18% HCl for 1440 min. The study observed that pore sizes between 500 µm and 600 µm resulted in the greatest osteoinduction, indicating a healthy balance between blood circulation and fluid flow in the human body. On the surface of the implant, rugae with a non-uniform microporous cell structure were also discovered. The mixture of NaOH and HCl could produce a Na-free oxide on the outer surface of the Ti implant, improving the bone-like apatite layer in SBF. These issues were investigated by Pattanayak *et al.* [137], and the results generally seem to support that a porosity of implant in the range of 55–75% massively promoted apatite formation on the samples after three days of immersion in SBF. However, after three weeks of implantation, the *in vivo* bioactivity showed no deleterious effects and signs of endochondral ossification.

Furthermore, Amin *et al.* [138] modified the porous surface implant on the femoral bone of male Wistar rats by combining acid-alkali treatment and heat treatment (AnH). It was proposed that the chemical composition of 18% HCl - 48% H_2SO_4 - 20% NaOH and 1 h of heat treatment at 600°C considerably enhanced biomechanical activity. In comparison to non-heat-treated surfaces, the nanotopographical characteristics of the Ti-6Al-4V surface encourage greater cell-implant interlocking and demonstrated more homogeneous cell distributions elongated on the surfaces. In contrast, the AnH method did not influence apatite formation and had no significant effect on cell attachment, proliferation, or the expression of osteogenic markers and its bioactivity was remarkably reduced after 21 days. Tsukanaka *et al.* [139] fabricated a porous SLM Ti-6Al-4V and diluted the sample in 20% NaOH and 18% HCl aqueous solution before heat treating the sample at 40 °C for 24 h. The results indicated that the SLM samples had a surface roughness value of around 24.58 µm and a high contact angle of 89.00°, suggesting their hydrophobic nature. The osteoblast attachment was tiny and spherical, as osteoblasts prefer rough surfaces with Ra values of around 3–5 µm. The ALP increased after two weeks, which coincides with antibodies to osteocalcin (OCN).

5. Surface modification of SLM Ti-6Al-4V

According to a study published by the Canadian Institute for Health Information, implant contamination, also known as Osteomyelitis (OM), is a severe problem in clinical applications and results in bone loss (osteolysis) [140]. The bone infection can develop from the inflammatory response to a microbial pathogen spreading through the bloodstream (hematogenous) towards a contiguous site [141,142]. The colonization of bacterium naturally

Table 4
Chemical Treatment to improve the surface roughness and pores of SLM-fabricated Ti-6Al-4V.

Ref	Year	Size (mm) (h × w × l)	Surface treatment	Duration (min)	[%] v/v of solution	Surface Pore size (μm)	Ra (μm)	Remarks
Fukuda *et al.*[136]	2011	Disc (3.3×15)	Alkali-acid treatment	1440	20% NaOH and 18% HCl	500–1200	–	Osteoinduction was observed at surface porosities of 500 and 600 μm.
Pattanayak *et al.*[137]	2011	Disc (6×15)	Alkali-acid treatment	180	20% NaOH and 18% HCl	400–800	–	Bone had infiltrated the pores and was directly attached to the walls after 12 weeks.
Bael *et al.*[126]	2012	Cube (6×6x12)	Acid etching	10	48% HF and 50% H_2O	1000	25.2	Cell adhesion was found to be highest on scaffolds with 500 μm pores.
De Wild *et al.*[124]	2013	Disc (6×7.5×3.8)	Acid treatment	15	32% HCl and 95% H_2SO_4	700	0.94–3.33	In sandblasted acid-etched scaffolds, bone was significantly increased.
Amin Yavari *etal.*[138]	2014	Disc (8×3)	Alkali- Acid treatment	60	20% NaOH, 18% HCl and 48% H_2SO_4	500	–	Apatite formed on the surface of an implant.
Xu *et al.*[125]	2016	Disc (1×10×10)	Acid treatment	15	36.5% HCl and 98% H_2SO_4	50–500	7.63–8.28	BIC% was nearly double on the SLM after the 8th week.
Tsukanaka *et al.*[139]	2016	Disc (1×14×14)	Alkali-acid treatment	1440	20% NaOH and 18% HCl	20–180	23.50	Bioactive treatment had a positive effect on osteoblast differentiation.
Wysocki *et al.*[127]	2016	Disc (6×4)	Acid Etching	3–9	2% HF and 20% HNO_3, 31.3HF and 9.0% HNO_3, 4.0% HF and 16% HNO_3, 2.2% HF and 20% HNO_3	200–500	–	The treated surface had a modulus close to that of compact bone. *In vitro* cell performance can be controlled to a certain extent by varying pore size.
Wang *et al.*[128]	2017	Cube (15 ×15 ×1)	Acid Etching	5	HF, H_2SO_4	–	6.02	The wettability and roughness of SLM-printed substrates were improved.
Balykin *et al.*[129]	2019	Disc (35×10×2)	Acid Etching	30, 60, 120	10%HF and 10%HNO_3	–	3.74–4.26	Cracks formed on the surface of SLM alloy after etching.
Thenard *et al.*[130]	2020	Disc (3×11.5)	Acid Etching	30	3% HF and 10% HNO_3	–	9.35–15.33	Roughness and the wetting of the surfaces were improved.
Jamshidi *et al.*[28]	2020	Dumbbell (6×70)	Acid Etching	10	1% HF 25% HNO_3 and 50% H_2O	–	6.6	HIP enhanced the cellular affinity of the surface and improved fatigue performance.
Vayssette *et al.*[131]	2020	Cube (120×120×19)	Acid Etching	15	48% HF, 13% HNO_3 and 10% H_2O	–	11.2	Surface roughness affects the SLM alloy's fatigue strength.
Le *et al.*[135]	2021	Disc (18×1)	Acid treatment	60	10.3% HCl and 6.3% H_2SO_4		43	MC3T3-E1 cells showed a tendency towards osteogenic differentiation.
Gonzalez *et al.*[134]	2021	Plate (10×10×10)	Acid treatment	8,20	67% HCl and 67% H_2SO_4		6.8–7.5	The presence of micropores and a thicker anatase layer improved levels of bioactivity.

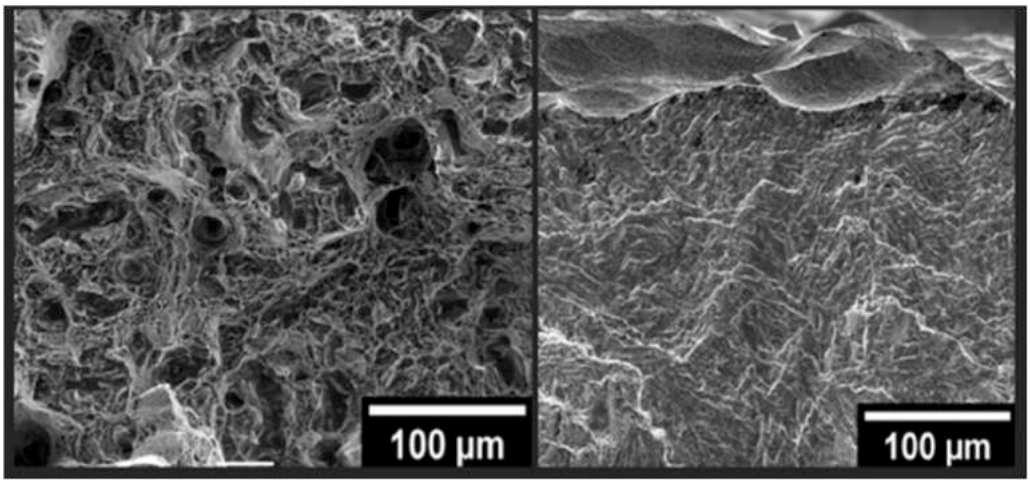

Fig. 11. Typical SEM images for (a) untreated and (b) treated with HF+HNO_3 for Ti-6Al-4V fabricated using SLM [28].

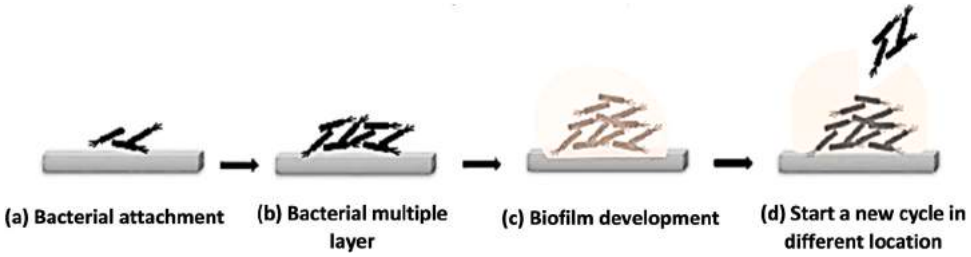

Fig. 12. The four stage of biofilm formation on a titanium plate after implantation [217].

happens as microbes bind on top of an implant surface to form a biofilm at the implantation site, as illustrated in Fig. 12. Biofilms commonly occur in four main stages. Fig. 12(a) shows the bacterium adhering to the surface, followed by replicating mitosis (Fig. 12(b)) in a microcolony formation. Then, the bacteria evolve and form biofilms, as seen in Fig. 12 (c). The bacterial pathogens emerged from the biofilm (Fig. 12(d)) and continually colonized a new region on the implant surface. Biofilms can resist environmental stress, especially antibiotics, making them a significant health problem in human microbial infections [142,143]. Therefore, unaddressed fracture infections can lead to loosening of an implant, which includes arthrodesis, amputations, and at times, death during the surgical procedures [144]. In reducing infections on the orthopedic implant, the use of surface coatings has been promoted [137,145].

Surface coating is an implant modification technique whereby materials are added with various thicknesses superficially on the implant surface. According to a prior study, silver nanoparticles (AgNPs) [146,147], silver nitrate ($AgNO_3$) [148], antibiotic, mesoporous bioactive glass (MBG) [149,150], bioactive glass (BG) [149], nitride [151,152], and hydroxyapatite [153] were all used in the coating of SLM Ti-6Al-4V. The coating processes for the base material are summarized in Table 5, which included spin coating, plasma electrolytic oxidation (PEO), immersion ion implantation, and chemical vapor deposition (CVD).

Several studies and reviews were conducted to investigate the use of antibiotics, particularly Ciprofloxacin®, to treat various bacterial illnesses, including skin and joint infections in adults [154,155]. Bacterial infection is a severe issue in implant surgery, particularly in the use of short-term biomedical devices. Under adverse conditions, the microbes overgrow and weaken the host immune system surrounding the implant. As a result, clinical infection occurs. The study presented by Vaithilingam *et al.* [156] evaluated the effect of the immobilized Ciprofloxacin® on SLM Ti-6Al-4V to minimize the risk of wound contamination during surgeries. The samples were initially polished to eliminate impurities before being coated for one hour using the immersion method. Surface wettability tests on the coated coupon revealed that the antibiotic was very stable and adhered to the sample surface under room circumstances. The antibacterial susceptibility of SLM Ti-6Al-4V was also evaluated by using *E.coli* and *S.aureus.* It was discovered that as immersion duration increased, Ciprofloxacin® molecules leached from the surface. The Ciprofloxacin® coating on SLM Ti-6Al-4V improved the therapeutic medication activity *in vitro* while decreasing orthopedic infection when implanted.

Several strategies were proposed to improve Ti implants with antibacterial capabilities. In particular, titanium coated with silver nanoparticles (AgNPs) has drawn much attention because of their broad antibacterial spectrum and ability to improve the implant surface. AgNPs were successfully employed in medical implants for infection control, preventing biofilm formation. Wang *et al.* [157] reported that the addition of AgNPs in Ti by using the plasma immersion ion implantation (PIII) method suggested that the implantable could inhibit bacterial growth and improve the reactive oxygen species (ROS) conductivity. This ROS induced the intracellular oxidation, membrane potential variation, and cellular activity of the implant. It indicated that the Ti coated with AgNPs had a higher density of AgNPs and decreased pH from 7.0 to 6.8, contributing to a higher antibacterial action than the uncoated sample. The oxidative stress caused by the changes in pH affected the division of the *S.aureus* membrane, thereby preventing biofilm formation. Hangel *et al.* [146] fabricated a porous implant with 3.75 times larger surface area than corresponding solid implants and embedded AgNPs in an oxide surface layer ranging in size between 7 nm and 25 nm by using PEO in a Ca/P-based electrolyte with a concentration of 3.0 g/l. Fig. 13 shows the cross-sectional morphology of the HA phase in the oxide layer of the porous implant. It can be seen that the oxide layer formed was uniform and the implant well covered with a diffusion layer beneath. The diffusion

Table 5
Surface coating method to reduce implant infections and toxicity.

Author, reference	Year	Size	Coating	Method	Duration	Test		Remarks
						In Vitro	*In Vivo*	
Vaithilingam *et al.*[156]	2014	Cube (10×10×3) mm	Ciprofloxacin®	immersion deposition	1 h	PBS		Improve wettability and antibacterial susceptibility.
Van Hangel *et al.*[146]	2017	4 cm	AgNPs	Electrolytic Oxidation	1 h	MSC	–	No presence of toxicity observed.
Shivaram *et al.*[148]	2017	Rods 3 mm	$AgNO_3$	Anodized surface electrodeposited	30 s and 3 min	–	Rat	Bone generation is not affected by silver coating.
Ye *et al.*[150]	2017	Cylinder (10×10) mm	(MBGs)	spin coating	10 s and 20 s	hBMSCs	–	Enhanced surface biofunctionalization for SLM Ti6A-4 V.
Yan *et al.*[153]	2017	–	HA	Immersion	7 and 14 days	SBF	–	2–5 μm spheroid particles formed on the surfaces.
Kao *et al.*[151]	2018	(15×1.25) mm	Carbon nitride (CN) and DLC (Ti-C:H)	(CFUMS)	– 340 V and a DC pulse frequency of 150 kHz.	Raw 264.7	–	Exhibited a good coating adhesion and highest wear resistance.
Zhao *et al.*[152]	2021	Cylinder (0.039, 0.097, 0.278 and 0.412) mm	Nitride	Annealing and gas nitriding	7 min	SBF	–	The wear mechanism of the nitride coating was brittle peeling.
Fazel *et al.*[147]	2021	–	AgNPs and HA	PEO	5 min	MC3T3-E1	–	HA coating sustained more antibacterial and metabolic activities.
Zhang *et al.*[149]	2021	Cylinder (5×10) mm	BG and MBG	Spin Coating	10 s and 20 s	–	Rabbit Femur	Significantly higher volumes of regenerated bone on MGB group implant.

Fig. 13. SEM images of microstructures formed by oxide layers [218].

oxide layer acts as an exchange membrane for the Ag^+ release between the SLM Ti-6Al-4V sample. There was a reduction in bacterial colony units, no cytotoxicity, and microbial activity found in antimicrobial assays compared to conventional Ti-6Al-4V.

Silver nitrate is an inorganic substance with the chemical formula $AgNO_3$ and is commonly used in clinical practice to cauterize infected tissues around a skin wound. In this regard, research has underway to use $AgNO_3$ as a bactericidal agent on the surfaces of SLM Ti-6Al-4V before implantation to hinder bacterial membrane adhesion. For example, electrochemical anodisation was used by Godoy Gallardo *et al.* [158] to encapsulate the thin $AgNO_3$ layer on the Ti-6Al-4V surface. The sample was biocompatible and antibacterial against microbial plagues like *Streptococcus sanguinis* and *Lactobacillus salivarius*. The higher concentration of $AgNO_3$ in the electrolyte increased the silver deposition on the titanium surface. The study mentioned that the $AgNO_3$ deposit showed no cytotoxicity in cell culture. In addition, Shivaram *et al.* [148] fabricated SLM Ti-6Al-4V with 25% porosity and immersed the samples in 0.1 M $AgNO_3$ at a constant voltage of 3 V for 3 mins electrodeposition. The silver released in the phosphate-buffered saline (PBS) solution was higher at 25% porosity than at 0% porosity, as indicated by the presence of porous surfaces. An excellent cell adhesion between the implant and the surrounding bone-tissue region was improved on the porous implant after being implanted for 12 weeks in male Sprague-Dawley rats. The cumulative release of the silver ion after implantation was within the toxic limit of 10 ppm (mg/ml).

Mesoporous bioactive glass (MBG) and bioactive glass (BG) are glass-based coatings that are well-known for their superior osteoinduction and osteostimulatory properties in cartilage regeneration. Ye *et al.* [150] and Zhang *et al.* [149] used spin coating at 500 rpm for the first 10 s followed by 2000 rpm for 20 s to coat the surface of SLM Ti-6Al-4V with bioactive glass. Then the implant's surface was then covered with MBG and BG, followed by heat treatment at rate of $1^\circ Cmin^{-1}$ until it reached 650°C and was held for 5 h. The results suggested that the MBG coating maintained the mesoporous structure and the chemical composition of the implant. *In vitro* study in human bone marrow stromal cells (hBMSCs) for seven days demonstrated that the hBMSCs spread well and showed numerous filopodia filament fibers on the implant surface. Zhang *et al.* [149] did *in vivo* tests on rabbit femoral condyles on MBG and BG SLM Ti-6Al-4V and demonstrated that the MBG coating enhanced osteoconduction and vascularization in bone defect healing after 9 weeks of implantation. The result was attributed to the Ca^{2+} and Si^{4+} emitted on the surface when implanted *in vivo*. However, MBG inherits brittleness, low bending strength, and fracture toughness in load-bearing applications due to its relatively poor mechanical properties.

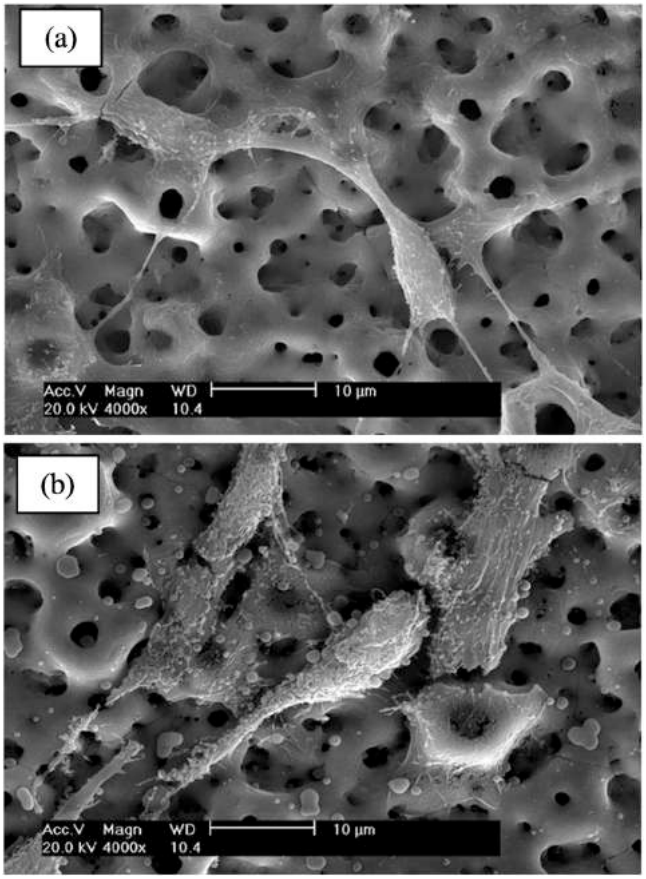

Fig. 14. The SEM images of the *S. aureus* bacteria adhered to the surface (a) Ag-free SLM (b) Ag-containing SLM[219].

Hydroxyapatite or HA, which has the same crystalline composition as the human body, is the most commonly used coating in load-bearing applications to enhance wound healing. Yan *et al.* [153] layered the SLM Ti-6Al-4V with biomimetic HA and tested its apatite-forming ability in SBF for seven days. The thickness of the precipitated HA layer increased continuously with the duration time of immersion in SBF. The Ca/P ratio of the HA layer formed was 1.68, close to the value for bone-like apatite. The morphological image results showed the growth of many spheroid cells with diameters of 2–5 µm on the surfaces after the SBF immersion. Fazel *et al.* [147] combined 2 g/l AgNPs and HA using the PEO method. The study demonstrated that the nano topography of the coated implant improved the antibacterial properties and metabolic activity against *S.aureus*. The SEM result for the *S.aureus* bacteria attached to the surface of SLM after 48 h of cell culture is presented in Fig. 14. Fig. 14(a) illustrates the *S.aureus* bacteria stacked on top of each other and colonized in the form of small clusters on the uncoated SLM sample. On the other hand, Fig. 14(b) shows the Ag-coated SLM Ti-6Al-4V, whereby the amount of *S.aureus* was smaller, indicating that the Ag^+ concentrations can efficiently suppress the growth of *S.aureus* on an Ag-coated sample. However, the coating of AgNPs only lasted for 8 h after *in vitro* cell culture. The surface of the HA sample formed spindle-like nanocrystals after 14 days of *in vitro* immersion in MC3T3 cell culture. These nanocrystals acted as the anchorage for cell growth and osteogenic differentiation on the surface of SLM Ti-6Al-4V implants.

Carbon nitride, C_3N_4 is a polymeric material that offers a low coefficient of friction, high wear resistance and good chemical inertness. A study by Kao *et al.* [151] evaluated the effect of SLM Ti-6Al-4V that coated with a thin film of carbon nitride (CN) and DLC-doped Ti (TieC:H) using closed field unbalanced magnetron sputtering (CFUMS). Cytotoxicity tests were conducted by using mouse leukemic monocyte-macrophage cells (Raw 264.7). It revealed that the cell density was highest on the coated surface rather than the non-nitrided counterpart. These findings confirmed that hydrophobic surfaces tend to induce a less favorable cell response due to lower protein absorption than hydrophilic carbon nitride (CN) surfaces. Zhao *et al.* [152] applied the nitride coating on the SLM Ti-6Al-4V by using annealing and gas nitriding at a temperature similarly Kao *et al.* [151]. From the study, Zhao *et al.* [152] demonstrated that the wear rate of the coated sample decreased from $18.27 \times 10-6\ mm^3/N{\cdot}m$ to $0.33 \times 10-6\ mm^3/N{\cdot}m$. This was caused by the brittle peeling of nitride on the SLM surface consisting of TiO_2, Ti_2O_3, SiO_2, and $CaCO_3$.

6. Corrosion resistance of SLM Ti-6Al-4V

Ti-6Al-4V is known as a stable metal and has higher corrosion resistance in seawater or atmospheric corrosion, due to the inhibition with a self-healing oxide film (TiO_2) at the surface, however easily dissolved in acidic conditions. Also, it has been proven that Ti-6Al-4V has high ferreting corrosion resistance as compared with other Ti-alloys with elements like Co, Cr and Mo.

The high cooling rate during the SLM powder bed fusion process results a variety of microstructures such as α'-martensite and fine grain formation, which differ from those produced by traditional processing technologies. These changes may have an impact on their mechanical properties as well as their corrosion resistance. Dai *et al.* [159] proved that the corrosion resistance of Ti-6Al-4V fabricated by SLM was lower than the Ti-6Al-4V Grade 5 alloy. The potentiodynamic measurements in the SLM Ti-6Al-4V were double that of conventional Ti-6Al-4V. This suggested that a large amount of acicular α' and fewer β phases originated from the high cooling rate during annealing possess inferior corrosion resistance. In addition, the corrosion resistance of the XZ-plane of the built-up Ti-6Al-4V alloy was lower than the XY-plane [160]. The close agreement of these findings was also suggested by Sharma *et al.* [161] when the SLM Ti-6Al-4V was immersed in several corrosive environments. Again, a combination between the higher metastable α′-martensite phase and surface porosity produced by the SLM part significantly decreased the corrosion resistance of the Ti-6Al-4V implant as compared to casting technology. Besides the surface porosity of the sample, Chi *et al.* [162] mentioned that corrosion rate was also increased with increasing surface roughness. The fast corrosion rate might easily oxidize and react with the human body fluid. In general, the pH of the human body ranges between 7.35 and 7.45. Even minor changes in pH can have serious consequences in the human body [163]. A previous study demonstrated that the corrosion of Ti-6Al-4V dental implant could interfere with the submucosal microbiome in the mouth caused by the changes of pH of the saliva [164]. The other changes related to corrosion include an increase in the number of anaerobic bacteria and inflammation through TLR-mediated recognition.

SLM Ti-6Al-4V has a higher α′ martensite phase with a low resistance to stress corrosion rate and easily crack in a high amount of oxygen due to a decrease in hardness. A heat treatment process could improve the Ti-alloy homogeneity by enhancing and stabilizing the β phase microstructure elements. It is expected that eliminating the fine α′ martensitic phase could improve the corrosion resistance of the SLM-produced alloy. Dai *et al.* [160] stated that α′ martensite is successfully removed, and the volume fraction of the β phase increases with the rising heat-treatment temperature. However, the corrosion resistance of SLM Ti-6Al-4V failed to improve despite the increase in the content of the β phase. Similarly, Pal *et al.* [165] suggested that heat treatment beyond the β-transus temperature equalized the microstructure of the main surface. In this study, samples were heated at 1015°C for 30 min at a rate of

10°C/min before being cooled to 750°C (rate of 10°C/min) for 2 h residence time, followed by the air circulation cooling in the furnace. However, as-fabricated samples have a higher potential to resist pitting corrosion as compared to heat-treated samples. In addition, Yan and co-authors [164] evaluated the effect of heat treatment by using vacuum annealing and hot isostatic pressing (HIP) on the corrosion properties of SLM Ti-6Al-4V. The HIP treatment resulted in the most significant corrosion resistance due to the combined action of β phase and zero porosity. This approach might provide a pristine surface, allowing for the formation of a dense oxide layer. Recently, the effect of a combination of post-heat treatment and anodisation with a platinum plate of Ti-6Al-4V implants on the corrosion behavior was reported by Longhitano *et al.* [166]. After the heat treatments process (ranging between 650 °C and 1050°C), the nucleation and growth of the β phase were increased. Further, an oxide film was obtained on the part surface, resulting in improved corrosion resistance and decreased ion release into the bloodstream. In general, heat treatment alone is not a great way to develop the corrosion resistance of Ti-6Al-4V alloys made by SLM. A proper heat treatment process should be investigated to improvising the corrosion resistance of the Ti-6Al-4V implant.

Many studies had previously shown that a fine-grained structure with a high grain boundary density serves as a location for passive film generation, resulting in an enhanced corrosion resistance. Besides, the repassivation process and surface treatment amongst the techniques could be implemented to reduce this alloy from degradation. Zhang *et al.* [167] soaked the specimens in the combination of different pH concentrations of sodium fluoride (NaF) and the artificial saliva to introduce the repassivation process on the Ti-6Al-4V surfaces. The corrosion resistance of Ti alloys increased as the NaF concentration increased, leading to the generation of repassive layers, but they still had significantly lower corrosion resistance than wrought Ti-6Al-4V. One of the critical parameters that affects the resistance to corrosion of implant alloys is the service surroundings. Qin *et al.* [168] studied the corrosion and passivation of SLM Ti-6Al-4V under different concentrations of NaCl and found that the oxide films of TiO, TiO_2, and Ti_2O_3 formed on the surface of the sample. The test samples were conducted in static and dynamic conditions. As the concentration of NaCl increased, the content of TiO_2 decreased, indicating worsened corrosion resistance as compared to the static condition. There were defects found on the sample under the dynamic condition as the Cl^- ions promote aggressive kinetic reactions with the oxide films, resulting in inferior corrosion resistance.

Over the past decade most research in SLM Ti-6Al-4V has emphasized the aid of ultrasonic technology to refine surface grain structure, emit residual stress, increase microhardness and ultimately enhance corrosion behavior. Zhang *et al.* [169] adopted an ultrasonic shot peening (USP) method by using 2.5 mm of 500 zirconia ball to treat the SLM Ti-6Al-4V surfaces. The microstructure of the SLM Ti-6Al-4V sample exhibited α' martensite and long β grains as the USP processing time increased. It also enhanced the microhardness, surface roughness, and potentially high corrosion resistance. Furthermore, Lu *et al.* [170] used a Q-switched Nd:YAG laser shot peening operating at 1 Hz and an irradiation wavelength of 1064 nm to treat SLM surfaces Ti-6Al-4V. This method promoted grain refinement in the surface layer and improved the Ti-alloy specimens' corrosion resistance.

Many attempts have been made to improve the mechanical properties and corrosion resistance of SLM implants by mixing the Ti-6Al-4V powder with various alloying metals as a part of their matrix composite during fabrication**.** Besides the materials like Niobium (Nb) being indicated as a barrier layer in medical applications[171], Tantalum (Ta) has also been recommended as an element for SLM Ti-6Al-4V due to its high β stabilizing elements and lower strength modulus [172]. Recently, Siu *et al.* [173] added 5 wt% of Nb particles into the Ti-6Al-4V powder and fabricated the sample by using SLM 125 HL machine. This novel alloy showed an outstanding corrosion resistance than the wrought Ti-6Al-4V, following potentiodynamic polarization testing. However, the yield strength and microhardness of the specimen were reduced due to the presence of a higher β phase, which was more ductile than the α' martensite phase. This study demonstrated that SLM Ti-6Al-4V-Nb was compatible with biomedical implants by tailoring the composition of Nb powder during product fabrication. Furthermore, Wang et al. [174] combined the alloying element of Nb in SLM Ti-6Al-4V processing to fabricate medical implants. They discovered that a 45% of Nb content was able to increase of tensile strength of the Ti-6Al-4V to 1030 MPa, more than 97% of the conventional sample. The samples were also tested in SBF solution, and it was discovered that the β phase in the SLM sample exhibited apatite formation on the surface. The amount of β phase in the sample increased as the Nb content increased. This study demonstrated that SLM Ti-Nb was compatible with biomedical implants and could enhance corrosion resistance. Currently, the evaluation of pure titanium that blend with Ta using SLM was reported by Sing et al. [175] but is still limited for SLM Ti-6Al-4V.

In summary, the corrosion behavior of SLM Ti-6Al-4V was closely related with the formation of α' martensite on the surface of the sample produced by rapid cooling during fabrication. Since heat treatment is currently unproven, it is crucial to focus on coating and combining SLM Ti-6Al-4V powder with a novel alloy to optimize implant corrosion behavior.

7. Challenges and the way forward

As stated in the previous sections, SLM Ti-6Al-4V cannot be fabricated to achieve a similar biological response to the human bone. Its strength remains above that of the strongest human cortical bone. For example, the current manufactured SLM Ti-6Al-4V (porosity: 63.21%; density: 1.63 $g{\cdot}cm^{-3}$), showed higher strength than for human cortical tibia and femur bones. Besides by using the common lattice structure like BCC, and FCC to meet the human bone properties, a topological optimization algorithm for the control of load transfer at the mimic bone-implant SLM Ti-6Al-4V contact could be worth developing. The geometrical modeling of the structure can be explored by using commercial finite element software such as Abaqus and Ansys. This optimal geometry can be evaluated by using the Von Mises failure criteria to validate the structural performance before being deployed as a biomedical implant.

The fabrication of Ti-6Al-4V lattices by SLM is still far from mature due to both the specific geometrical complexity and the strict conditions for fabricating the quality of a strut. The same concern applies to the lattices, which concentrate most in small areas and defects during axial loading. In this regard, SLM parameters that can realize the optimal build geometry with the desired quality should be developed. This means that pores and lack-of-fusion defects are unavoidable in the struts. The use of pore-free feedstock powder is expected to reduce internal porosity. Through careful control of the SLM process, it is also possible to minimize the presence of lack-of-fusion defects. In addition, there exists a significant lack of design tools specifically for the design of patient-specific implants. Due to this restriction, manual intervention and suboptimal design approaches are required, which adds unnecessary complexity, risk and cost to the production of SLM implants. To promote and improve the manufacturability of SLM Ti-6Al-4V, methods to optimize the skeletonization in the topological design via the minimum size of the struts and simultaneously regulating the number of holes need to be developed**.**

The size and void formation of the SLM Ti-6Al-4V part significantly lowered its tensile performance. Both factors can be manipulated by controlling the input parameters during the SLM process. The hatching distance, laser power, scan speed, hatch spacing and layer thickness need to be carefully addressed. The design

of experimental studies could be enhanced through the use of optimization techniques such as Taguchi and the response surface method.

Less tensile property data was reported on SLM Ti-6Al-4V lattices due to their rough strut surfaces, internal defects and incompletely decomposed α′-martensitic microstructure, which together eliminated tensile ductility. In general, brittle fracture remains a significant concern for the wider applications of SLM Ti-6Al-4V and needs to be appropriately addressed before implantation in human bone. Post-SLM treatment may improve ductility through controlling the rate of cooling.

7.1. Cavity size manufactured by using SLM and biomedical needs

The minimum cavity size that can be manufactured in an SLM Ti-6Al-4V lattice is about 100 µm[176], higher than most cavities in human bone. This discrepancy limits the manufacture of more biomimetic implants. Researchers have concluded that pore size in the range of 400–600 µm is optimal for (i) the expression and production of collagen and aggrecan, (ii) supplying oxygen from blood vessels to neighboring cells, and (iii) enhancing bone formation and the mechanical properties of cartilage. The larger size range (400–600 µm) of pores is more suitable for both angiogenesis and bone ingrowth. In either case, it is demanding for the current SLM production techniques. One latent risk of manufacturing small cavities by SLM is how to remove the unmelted powder particles on the sample. These particles may have to stay in the lattice, and thus there is a risk of them entering the patient's body.

Emerging evidence has confirmed the crucial role of micro-and nanoscale porous structures in regulating cell morphology, adhesion, differentiation, migration, and proliferation. One unique opportunity to produce lattices with a hierarchical porous structure is to combine SLM with dealloying [177]. Recent innovations by using molten metals as the dissolution medium provided a generic method of manufacturing nano-porous materials from nearly any metal, for example, Ti, Ta, Nb and Cr [178–180]. The integration of SLM and dealloying has the potential to produce hierarchical porous structures that replicate the properties of human bones at macro-to-nano scales [181]. The effect of dealloying on an implant mechanical properties is yet to be quantified.

7.2. SLM Ti-6Al-4V structures with bioactive surfaces

The surface of an SLM Ti-6Al-4V lattice is bio-inert and the survival of cells on it can be an issue, in addition to bacterial infection. It has been shown that surface treatment with HCl and NaOH can improve the biological activity of SLM Ti-6Al-4V lattice implants, leading to easier fixation around the concerned bone and improving long-term stability [182]. The coating is another option to enhance vascularization and osseointegration [183]. The antibacterial properties of SLM Ti-6Al-4V lattice implants could be improved by introducing silver, nanoparticles or antihistamine [25,184–186]. These coatings are known to protect the implant from infection of broad spectrum bacteria without degrading the properties of the implant. However, the surface coating can cause leaching on the surface of the implant, thereby decreasing the implant integrity. It is great to obtain access to a novel exploration.

7.3. Novel β-titanium alloys for lattice implants

A wide variety of Al-, V- and Ni-free new β-Ti alloys were developed for biomedical applications over the last two decades [16]. They were more biocompatible than Ti-6Al-4V and possess a lower Young's modulus. In addition, some of them offered good shape memory or super-elasticity. A recent study had reported good mechanical properties for SLM β-Ti alloys [187]. They represent a new class of titanium lattice materials that can enhance both the mechanical and biological performance of AM implants. Challenges lie in how to translate their unique properties into lattice forms.

8. Applications of SLM Ti-6Al-4V

Biomodelling (the creation of tangible models of the human body for surgical planning and testing), the design and production of personalized implants for prosthetic procedures, rehabilitation and tissue engineering are all examples of clinical applications of AM. It is observed that porous Ti-6Al-4V can have properties close to those of human bone, which indicates that SLM has a great potential to produce complex shapes and show excellent cell adhesion in both *in vivo* and *in vitro* cell cultures. At the same time, this can fulfill the critical requirement essential to enhance the longevity of the bones in human bodies. Simulation models of human tissues and bones can be produced in advance by using AM printing technology, allowing surgeons to rehearse operating techniques in advance, resulting in actual surgical operations that are more accurate and safer.

At present, SLM printed biomaterials are mainly used to produce implants for tissue repair, dentistry and orthopedics, and surgical tools as illustrated in Fig. 15**.** One of the major applications used in orthopedic applications for SLM fabricated Ti-6Al-4V is for fracture plates. SLM, which has the advantage of tailoring bone and fixation type, can be used in fracture fixation. Surgeons prefer SLM Ti-6Al-4V, which is lightweight and MRI compatible as it is easier to handle during surgery. Internal implants or plates are the most common fixations for fractures, whereby it mimics the bone structure. Therefore, by using SLM Ti-6Al-4V it can reduce the production time, cost and feedstock required. SLM Ti-6A-4 V can also be used in external fixators e.g. Ilizarov frames. The current price of titanium made for the external fixator market is costly and requires a lot of feedstock. SLM allows for the rapid preparation of more detailed designs for specific bone distortions, such as multiplanar distortions, and for the treatment of axis distortion in young children.

As illustrated in Fig. 15(b), the surgical guide by using k-wire serves as a guide for the appropriate osteotomy before drilling for the implantation of plates. The surgical guide can be used for both orthopedic implants and in dentistry. In dentistry, the surgical guide acts as a guide for optimal position of dental implant for optimal placement in final placement of the implants [188]. For maxillofacial surgeries, SLM Ti-6Al-4V is a great option before applying dental braces, especially for people with jaw or underbite problems. This can reduce the operation cost before brace application.

Another consideration for further applications of SLM Ti-6Al-4V is for a cranial prosthesis as shown in Fig. 15(a) [189,190]. This is the most expensive replacement in the current market as the design needs to be tailored to the exact demands of the patient's cranial size and shape [191]. The cost-effectiveness of SLM Ti-6Al-4V can reduce the market price of the available skull replacement. The scapula prosthesis illustrated in Fig. 15(c) is an orthopedic implant that needs to be tailored based on human anatomy. The scapula is a flat human bone that can fracture under stress or sudden inertia [192,193]. As shown in Fig. 15(d), the knee prosthesis is known as knee arthroplasty and mostly performed for osteoarthritis and other knee diseases such as rheumatoid arthritis amongst elderly patients [194]. SLM Ti-6Al-4V can be utilized for arthroplasty due to its good mechanical properties and wear and tear resistance as these implantation types experience friction during every movement [194,195].

SLM Ti-6Al-4V implants enhance joints in total joint replacement surgery as illustrated in Fig. 15(g) and Fig. 15(h). For a total hip joint replacement, the component includes an acetabular cup (Fig. 15(g)) and a femoral hip stem (Fig. 15(h)). The acetabular cup fits inside the hip bone and the hip prosthesis is connected to it. Problems that have been associated with total hip replacement involve loosening

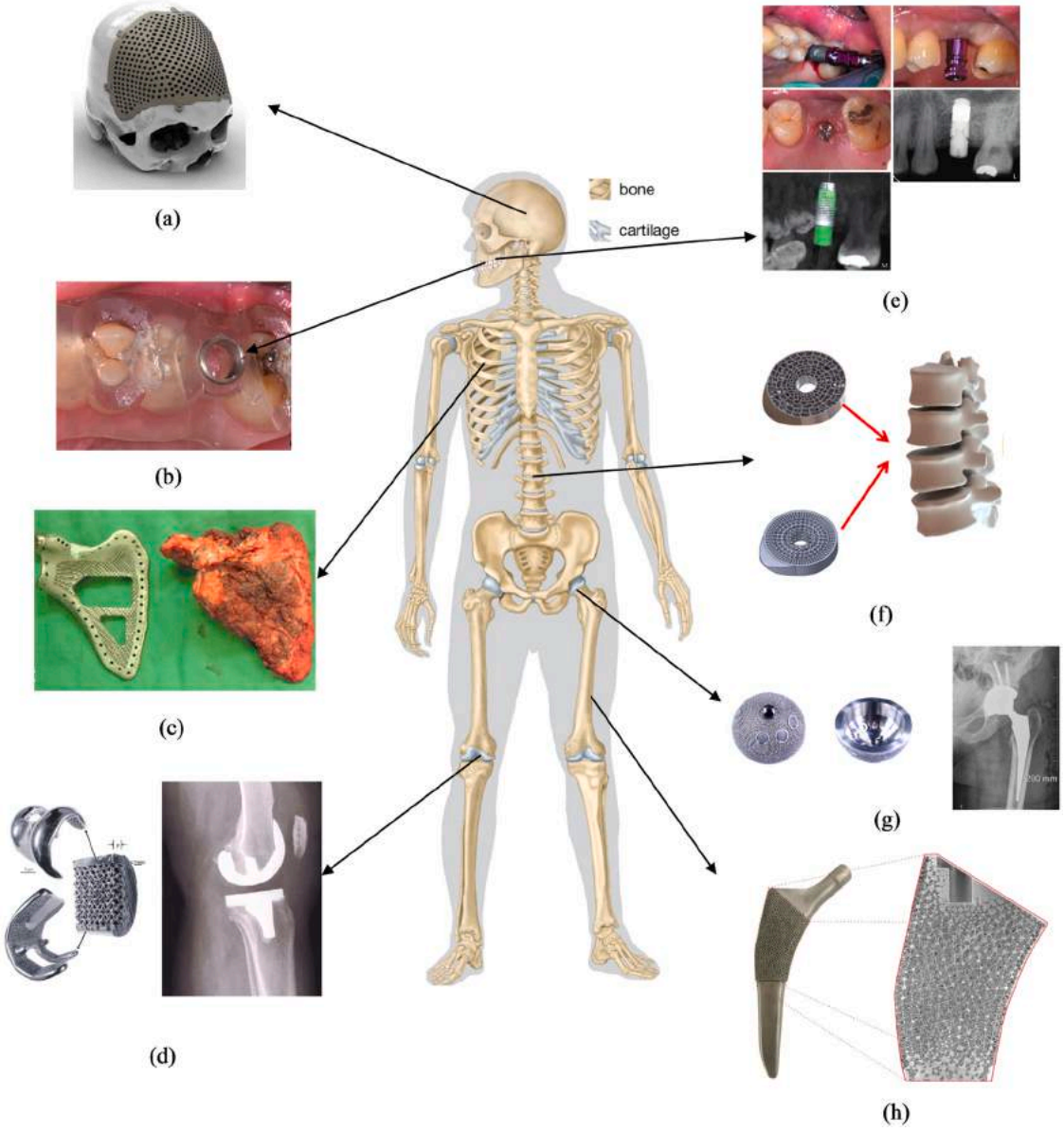

Fig. 15. The biomedical application of 3D printing of SLM Ti-6Al-4V includes (a) cranial prosthesis[221]; (b) surgical guide[222]; (c) scapula prosthesis[221]; (d) knee prosthesis [223]; (e) dental implants[222]; (f) interbody fusion cage[223]; (g) acetabular cup[223]; and (h) hip prosthesis[224].

or dislocation of the acetabular cup and the tissue irritation due to metal debris. These issues commonly result in infections and discomfort for the patient, and thus require additional surgery [196,197]. The interbody fusion cage Fig. 15(f) is a hollow cylinder made of some type of metal, usually, titanium, which serves as a space holder between the disc of the vertebrae, which eventually become part of the spine [198]. They are widely used to treat degenerative lumbar spinal diseases and stabilize the adjacent vertebra [199]. The SLM fabricated interbody cage fusion can improve the threaded hole of the cage fusion, improving the compression and preventing the loosening of screws after implantation. Nevertheless, technological advancements in AM have enabled research into the upgrading of hip components, with an emphasis on the bearing surfaces and the biocompatibility of the parts.

Anterior cruciate ligament (ACL) damage, a typical sports injury, continues to rise, particularly amongst young and active patients [200]. SLM Ti-6Al-4V, based on the study, can be used to create custom guides to aid in placement of the femoral head during the ACL reconstruction as the complexity revision rate of ACL is as high as 35% for patients of age 20 years and above [201]. A bone scaffold or bone graft, which refers to the biomaterial structure,are used for bone defect reconstruction. SLM Ti-6Al-4V can be used for bone scaffold engineering in generating the bone while delivering the therapeutic molecules locally to the site of action [202]. Based on previous studies, scaffolds with 200 µm pores exhibited the highest cell adhesion when produced from SLM Ti-6Al-4V [59]. In the field of biomaterials, SLM Ti-6Al-4V can play a critical role in complex tissue engineering, especially for the regeneration of bone tissues. The standard autograft and allograph currently available in the market lead to pain, infection, scarring, blood loss and can cause an immune response [203].

For load-bearing, especially in orthopedic applications, multiple compression, tension, bending and torsion are applied when patients move. This scenario is critical for SLM fabricated Ti-6Al-4V. Furthermore, recycling and reusing the metallic materials produced from SLM Ti-6Al-4V can reduce the cost to both the patient and the health industry. Further studies are still needed to improve the reliability of SLM parts, including preventing unfavorable effects caused by SLM improving surface roughness and cell adhesion.

9. Conclusions

Due to their biocompatibility and non-toxicity with compact bone, SLM Ti-6Al-4V implants are developed and applied in various medical procedures. Lowering the stress-shielding effect, surface modification and treatment may broaden the potential use of SLM Ti-6Al-4V to treat bone disorders, particularly in functional movement and load-bearing skeletal muscle applications.

The SLM Ti-6Al-4V lattice structure has a reduced stress-shielding effect and is equivalent to cortical and cancellous bone. It has been demonstrated that structural porosity ranging from 65% to 75% demonstrates higher osteogenic activity close to that of real bone and makes these structures good for allowing tissue ingrowth. In addition, built-up SLM Ti-6Al-4V yielded Ra value of approximately 5 µm. Here, chemical treatment such as with HNO_3, HCl, H_2SO_4 and HF can remove the film of oxide on the implant's surface and provides an appropriate Ra of 1–2 µm for the anchorage of growth cells. Chemical treatment of SLM Ti-6Al-4V deals with minor surface scratches, cleanly ablates metallic globule aggregates and repairs surface cracks, reducing the Ra of the SLM sample. However, strong acid such as HF and H_2SO_4 can lead to cracks and corrosion on the surface of implant. The heat treatment and surface treatment such as NaF and NaCl can improve the corrosion resistance of SLM Ti-6Al-4V. Alloying the SLM Ti-6Al-4V with Ta and Nb simultaneously increases the amount of β phase, increasing the mechanical properties and corrosion resistance.

Furthermore, inadequate melting results in low-quality products with a porous structure and low mechanical strength that cannot be utilized for biomedical implants. On the other hand, the surface coating enhances bone regeneration and increases the attachment of osteoblasts and osteoclast cells. The formation of TiO_2 on the surface exhibits better osseointegration and reduces bacterial infection of *Streptococcus sanguinis* and *Lactobacillus salivarius* without jeopardizing the implant efficiency. The *in vivo* and *in vitro* testing can assess the bone ingrowth and integration at the bioactive surface for the apatite and cells on the surface. The increase in HA nanocrystals acts as the anchorage for growth cells and osteogenic differentiation on the surface of SLM Ti-6Al-4V implants, which determines implant biocompatibility. Therefore, the combined surface treatment and modification are advanced methods of treating SLM Ti-6Al-4V for biomedical applications.

This review demonstrates the translational potentials and uses of SLM Ti-6Al-4V orthopedic implants to improve patient well-being for fracture fixing and osteoplasty. It also explored a systematic strategy and direction for future additive manufacture of implants while enhancing osseointegration and out performing traditional orthopedic implants on the market. By identifying the chemical, physical and biological limitations of SLM Ti-6Al-4V, appropriate SLM Ti-6Al-4V implants can be expanded for numerous clinical indications apart from fracture fixation in such as in form of lattice structure, compatible to human anatomical. Further work focussing on the weak bonding between the fracture sites and SLM implants and the resultant poisoning in the human body will be crucial and likely to yield interesting discoveries.

Declaration of Competing Interest

The authors declare that they have no known competing financial interests or personal relationships that could have appeared to influence the work reported in this paper.

Acknowledgments

This research was funded by Universiti Teknologi Malaysia with "Geran Universiti Penyelidik' UTMFR Scheme Q.K.130000.2656.21H13 and Ministry of Higher Education (MOHE) with Fundamental Research Grant (FRGS) Scheme FRGS/**1/2020/TK0/UTM/02/59** financial support provided throughout the course of this research project.

References

[1] K.P. Cowan PT, Anatomy, Bones, in, StatPearls Publishing, 2020,
[2] R. Florencio-Silva, G.Rd.S. Sasso, E. Sasso-Cerri, M.J. Simões, P.S. Cerri, Biology of bone tissue: structure, function, and factors that influence bone cells, Biomed. Res. Int. 2015 (2015) 421746, https://doi.org/10.1155/2015/421746
[3] A. Terashima, H. Takayanagi, The role of bone cells in immune regulation during the course of infection, Semin. Immunopathol. 41 (2019) 619–626, https://doi.org/10.1007/s00281-019-00755-2
[4] D. Martin, E. Gormley-Fleming, The skeletal system, Fundamentals of Children and Young People's Anatomy and Physiology: A Textbook for Nursing and Healthcare Students, (2021).
[5] P.T. Cowan, P. Kahai, Anatomy, Bones, (2019).
[6] M.S. Ghiasi, J. Chen, A. Vaziri, E.K. Rodriguez, A. Nazarian, Bone fracture healing in mechanobiological modeling: a review of principles and methods, Bone Rep. 6 (2017) 87–100, https://doi.org/10.1016/j.bonr.2017.03.002
[7] C.S. Bahney, R.L. Zondervan, P. Allison, A. Theologis, J.W. Ashley, J. Ahn, T. Miclau, R.S. Marcucio, K.D. Hankenson, Cellular biology of fracture healing, J. Orthop. Res. 37 (2019) 35–50, https://doi.org/10.1002/jor.24170
[8] D.O. Verbeek, J.P. van der List, C.M. Tissue, D.L. Helfet, Predictors for long-term hip survivorship following acetabular fracture surgery: importance of gap compared with step displacement, J. Bone Jt. Surg. Am. 100 (2018) 922–929, https://doi.org/10.2106/jbjs.17.00692
[9] T. Ono, H. Takayanagi, Osteoimmunology in bone fracture healing, Curr. Osteoporos. Rep. 15 (2017) 367–375, https://doi.org/10.1007/s11914-017-0381-0
[10] D. Clark, M. Nakamura, T. Miclau, R. Marcucio, Effects of aging on fracture healing, Curr. Osteoporos. Rep. 15 (2017) 601–608, https://doi.org/10.1007/s11914-017-0413-9
[11] G.D. Revankar, R. Shetty, S.S. Rao, V.N. Gaitonde, Wear resistance enhancement of titanium alloy (Ti-6Al-4V) by ball burnishing process, J. Mater. Res. Technol. 6 (2017) 13–32, https://doi.org/10.1016/j.jmrt.2016.03.007
[12] A.J.T. Teo, A. Mishra, I. Park, Y.J. Kim, W.T. Park, Y.J. Yoon, Polymeric biomaterials for medical implants and devices, ACS Biomater. Sci. Eng. 2 (2016) 454–472, https://doi.org/10.1021/acsbiomaterials.5b00429
[13] G. Soon, B. Pingguan-Murphy, K.W. Lai, S.A. Akbar, Review of zirconia-based bioceramic: surface modification and cellular response, Ceram. Int. 42 (2016) 12543–12555, https://doi.org/10.1016/j.ceramint.2016.05.077
[14] F.A. Shah, P. Thomsen, A. Palmquist, Osseointegration and current interpretations of the bone-implant interface, Acta Biomater. 84 (2019) 1–15, https://doi.org/10.1016/j.actbio.2018.11.018
[15] C.S. Bahney, R.L. Zondervan, P. Allison, A. Theologis, J.W. Ashley, J. Ahn, T. Miclau, R.S. Marcucio, K.D. Hankenson, Cellular biology of fracture healing, J. Orthop. Res. 37 (2019) 35–50.
[16] L.C. Zhang, L.Y. Chen, A review on biomedical titanium alloys: recent progress and prospect, Adv. Eng. Mater. 21 (2019) 1–29, https://doi.org/10.1002/adem.201801215
[17] L.C. Zhang, L.Y. Chen, L. Wang, Surface modification of titanium and titanium alloys: technologies, developments, and future interests, Adv. Eng. Mater. 22 (2020) 1–37, https://doi.org/10.1002/adem.201901258
[18] X. Wang, S. Xu, S. Zhou, W. Xu, M. Leary, P. Choong, M. Qian, M. Brandt, Y.M. Xie, Topological design and additive manufacturing of porous metals for bone scaffolds and orthopaedic implants: a review, Biomaterials 83 (2016) 127–141, https://doi.org/10.1016/j.biomaterials.2016.01.012
[19] Y.-H. Kim, M. Choi, J.-W. Kim, Are titanium implants actually safe for magnetic resonance imaging examinations? Arch. Plast. Surg. 46 (2019) 96–97, https://doi.org/10.5999/aps.2018.01466
[20] K. Iwatsuki, H. Yoneda, T. Onishi, H. Ishii, S. Kurimoto, M. Yamamoto, M. Tatebe, H. Hirata, Compatibility of magnetic resonance imaging in patients with orthopedic implants: manufacturer questionnaires, Nagoya J. Med. Sci. 82 (2020) 79–84, https://doi.org/10.18999/nagjms.82.1.79
[21] M. Rizwan, M. Hamdi, W. Basirun, Bioglass® 45S5–based composites for bone tissue engineering and functional applications, J. Biomed. Mater. Res. A 105 (2017) 3197–3223, https://doi.org/10.1002/jbm.a.36156
[22] A. Szcześ, L. Hołysz, E. Chibowski, Synthesis of hydroxyapatite for biomedical applications, Adv. Colloid Interface Sci. 249 (2017) 321–330, https://doi.org/10.1016/j.cis.2017.04.007
[23] S. Zhang, Hydroxyapatite Coatings for Biomedical Applications, Taylor & Francis, 2013.
[24] M. Plewinski, K. Schickle, M. Lindner, A. Kirsten, M. Weber, H. Fischer, The effect of crystallization of bioactive bioglass 45S5 on apatite formation and degradation, Dent. Mater. 29 (2013) 1256–1264, https://doi.org/10.1016/j.dental.2013.09.016
[25] A. Myakinin, A. Turlybekuly, A. Pogrebnjak, A. Mirek, M. Bechelany, I. Liubchak, O. Oleshko, Y. Husak, V. Korniienko, K. Lesniak-Ziolkowska, D. Dogadkin, R. Banasiuk, R. Moskalenko, M. Pogorielov, W. Simka, In vitro evaluation of electrochemically bioactivated Ti6Al4V 3D porous scaffolds, Mater. Sci. Eng. C Mater. Biol. Appl. 121 (2021) 111870, https://doi.org/10.1016/j.msec.2021.111870
[26] E.H. Valente, M.S. Jellesen, M.A.J. Somers, T.L. Christiansen, Gaseous surface hardening of Ti-6Al-4V fabricated by selective laser melting, Surf. Coat. Technol. 383 (2020), https://doi.org/10.1016/j.surfcoat.2019.125278

[27] Z.J. Wally, A.M. Haque, A. Feteira, F. Claeyssens, R. Goodall, G.C. Reilly, Selective laser melting processed Ti6Al4V lattices with graded porosities for dental applications, J. Mech. Behav. Biomed. Mater. 90 (2019) 20–29, https://doi.org/10.1016/j.jmbbm.2018.08.047

[28] P. Jamshidi, M. Aristizabal, W. Kong, V. Villapun, S.C. Cox, L.M. Grover, M.M. Attallah, Selective laser melting of Ti-6Al-4V: the impact of post-processing on the tensile, fatigue and biological properties for medical implant applications, Mater 13 (2020), https://doi.org/10.3390/ma13122813

[29] A.N. Aufa, M.Z. Hassan, Z. Ismail, The fabrication of titanium alloy biomedical implants using additive manufacturing: a way forward, J. Met. Mater. Min. 7 (2021) 39–48, https://doi.org/10.31437/2414-2115.2021.07.5

[30] H. Fakhr Nabavi, M. Aliofkhazraei, Morphology, composition and electrochemical properties of bioactive-TiO2/HA on CP-Ti and Ti6Al4V substrates fabricated by alkali treatment of hybrid plasma electrolytic oxidation process (estimation of porosity from EIS results), Surf. Coat. Technol. 375 (2019) 266–291, https://doi.org/10.1016/j.surfcoat.2019.07.032

[31] M.S. Tareq, T. Rahman, M. Hossain, P. Dorrington, Additive manufacturing and the COVID-19 challenges: an in-depth study, J. Manuf. Syst. (2021).

[32] S. Ghods, E. Schultz, C. Wisdom, R. Schur, R. Pahuja, A. Montelione, D. Arola, M. Ramulu, Electron beam additive manufacturing of Ti6Al4V: Evolution of powder morphology and part microstructure with powder reuse, Materialia 9 (2020) 100631.

[33] D. Bourell, J.P. Kruth, M. Leu, G. Levy, D. Rosen, A.M. Beese, A. Clare, Materials for additive manufacturing, CIRP Ann. Manuf. Technol. 66 (2017) 659–681, https://doi.org/10.1016/j.cirp.2017.05.009

[34] S.C. Ligon, R. Liska, J. Stampfl, M. Gurr, R. Mülhaupt, Polymers for 3D printing and customized additive manufacturing, Chem. Rev. 117 (2017) 10212–10290, https://doi.org/10.1021/acs.chemrev.7b00074

[35] M. Attaran, The rise of 3-D printing: the advantages of additive manufacturing over traditional manufacturing, Bus. Horiz. 60 (2017) 677–688, https://doi.org/10.1016/j.bushor.2017.05.011

[36] S.A.M. Tofail, E.P. Koumoulos, A. Bandyopadhyay, S. Bose, L. O'Donoghue, C. Charitidis, Additive manufacturing: scientific and technological challenges, market uptake and opportunities, Mater. Today 21 (2018) 22–37, https://doi.org/10.1016/j.mattod.2017.07.001

[37] L.C. Zhang, H. Attar, Selective laser melting of titanium alloys and titanium matrix composites for biomedical applications: a review, Adv. Eng. Mater. 18 (2016) 463–475.

[38] P.K. Gokuldoss, S. Kolla, J. Eckert, Additive manufacturing processes: Selective laser melting, electron beam melting and binder jetting-selection guidelines, Materials 10 (2017), https://doi.org/10.3390/ma10060672

[39] Q. Wang, P. Zhou, S. Liu, S. Attarilar, R.L.W. Ma, Y. Zhong, L. Wang, Multi-scale surface treatments of titanium implants for rapid osseointegration: a review, Nanomaterials 10 (2020) 1–27, https://doi.org/10.3390/nano10061244

[40] A.A. Zadpoor, J. Malda, Additive MAnufacturing of Biomaterials, Tissues, and Organs, Ann. Biomed. Eng. 45 (2017) 1–11, https://doi.org/10.1007/s10439-016-1719-y

[41] S. Bagehorn, J. Wehr, H.J. Maier, Application of mechanical surface finishing processes for roughness reduction and fatigue improvement of additively manufactured Ti-6Al-4V parts, Int. J. Fatigue 102 (2017) 135–142, https://doi.org/10.1016/j.ijfatigue.2017.05.008

[42] Y. Bai, Y. Yang, D. Wang, M. Zhang, Influence mechanism of parameters process and mechanical properties evolution mechanism of maraging steel 300 by selective laser melting Materials Science & Engineering A In fl uence mechanism of parameters process and mechanical properties evolution mech, Mater. Sci. Eng. A 703 (2017) 116–123, https://doi.org/10.1016/j.msea.2017.06.033

[43] Y. Zhai, H. Galarraga, D.A. Lados, Microstructure, static properties, and fatigue crack growth mechanisms in Ti-6Al-4V fabricated by additive manufacturing: LENS and EBM, Eng. Fail. Anal. 69 (2016) 3–14, https://doi.org/10.1016/j.engfailanal.2016.05.036

[44] I. Polozov, V. Sufiiarov, A. Popovich, D. Masaylo, A. Grigoriev, Synthesis of Ti-5Al, Ti-6Al-7Nb, and Ti-22Al-25Nb alloys from elemental powders using powder-bed fusion additive manufacturing, J. Alloy. Compd. 763 (2018) 436–445, https://doi.org/10.1016/j.jallcom.2018.05.325

[45] X. Shen, P. Shukla, A.K. Subramaniyan, A. Zammit, P. Swanson, J. Lawrence, M.E. Fitzpatrick, Residual stresses induced by laser shock peening in orthopaedic Ti-6Al-7Nb alloy, Opt. Laser Technol. 131 (2020) 106446, https://doi.org/10.1016/j.optlastec.2020.106446

[46] H. Shipley, D. McDonnell, M. Culleton, R. Coull, R. Lupoi, G. O'Donnell, D. Trimble, Optimisation of process parameters to address fundamental challenges during selective laser melting of Ti-6Al-4V: A review, Int. J. Mach. Tools Manuf. 128 (2018) 1–20, https://doi.org/10.1016/j.ijmachtools.2018.01.003

[47] A. Khorasani, I. Gibson, U.S. Awan, A. Ghaderi, The effect of SLM process parameters on density, hardness, tensile strength and surface quality of Ti-6Al-4V, Addit. Manuf. 25 (2019) 176–186, https://doi.org/10.1016/j.addma.2018.09.002

[48] Y. Hu, S. Wu, P. Withers, J. Zhang, H. Bao, Y. Fu, G. Kang, The effect of manufacturing defects on the fatigue life of selective laser melted Ti-6Al-4V structures, Mater. Des. 192 (2020) 108708, https://doi.org/10.1016/j.matdes.2020.108708

[49] P. Qin, Y. Chen, Y.-J. Liu, J. Zhang, L.-Y. Chen, Y. Li, X. Zhang, C. Cao, H. Sun, L.-C. Zhang, Resemblance in corrosion behavior of selective laser melted and traditional monolithic β Ti-24Nb-4Zr-8Sn alloy, ACS Biomater. Sci. Eng. 5 (2018) 1141–1149, https://doi.org/10.1021/acsbiomaterials.8b01341

[50] C. Yang, Z. Zhang, S. Li, Y. Liu, T. Sercombe, W. Hou, P. Zhang, Y. Zhu, Y. Hao, Z. Zhang, Simultaneous improvement in strength and plasticity of Ti-24Nb-4Zr-8Sn manufactured by selective laser melting, Mater. Des. 157 (2018) 52–59, https://doi.org/10.1016/j.matdes.2018.07.036

[51] X. Zhan, S. Li, Y. Cui, A. Tao, C. Wang, H. Li, L. Zhang, H. Yu, J. Jiang, C. Li, Comparison of the osteoblastic activity of low elastic modulus Ti-24Nb-4Zr-8Sn alloy and pure titanium modified by physical and chemical methods, Mater. Sci. Eng. C 113 (2020) 111018, https://doi.org/10.1016/j.msec.2020.111018

[52] L.C. Zhang, D. Klemm, J. Eckert, Y.L. Hao, T.B. Sercombe, Manufacture by selective laser melting and mechanical behavior of a biomedical Ti–24Nb–4Zr–8Sn alloy, Scr. Mater. 65 (2011) 21–24, https://doi.org/10.1016/j.scriptamat.2011.03.024

[53] M. Zhang, C. Chen, C. Liu, S. Wang, Study on porous Mg-Zn-Zr ZK61 alloys produced by laser additive manufacturing, Metals 8 (2018) 635, https://doi.org/10.3390/met8080635

[54] L.-Y. Chen, Y.-W. Cui, L.-C. Zhang, Recent development in beta titanium alloys for biomedical applications, Metals 10 (2020) 1139, https://doi.org/10.3390/met10091139

[55] T. Vilaro, C. Colin, J.D. Bartout, As-fabricated and heat-treated microstructures of the Ti-6Al-4V alloy processed by selective laser melting, Metall. Mater. Trans. A 42 (2011) 3190–3199, https://doi.org/10.1007/s11661-011-0731-y

[56] N. Biswas, J.L. Ding, V.K. Balla, D.P. Field, A. Bandyopadhyay, Deformation and fracture behavior of laser processed dense and porous Ti6Al4V alloy under static and dynamic loading, Mater. Sci. Eng. A 549 (2012) 213–221, https://doi.org/10.1016/j.msea.2012.04.036

[57] P.-H. Li, W.-G. Guo, W.-D. Huang, Y. Su, X. Lin, K.-B. Yuan, Thermomechanical response of 3D laser-deposited Ti–6Al–4V alloy over a wide range of strain rates and temperatures, Mater. Sci. Eng. A 647 (2015) 34–42, https://doi.org/10.1016/j.msea.2015.08.043

[58] G. Kasperovich, J. Hausmann, Improvement of fatigue resistance and ductility of TiAl6V4 processed by selective laser melting, J. Mater. Process. Technol. 220 (2015) 202–214, https://doi.org/10.1016/j.jmatprotec.2015.01.025

[59] B. Wysocki, J. Idaszek, J. Zdunek, K. Rozniatowski, M. Pisarek, A. Yamamoto, W. Swieszkowski, The influence of selective laser melting (SLM) process parameters on in-vitro cell response, Int. J. Mol. Sci. 19 (2018), https://doi.org/10.3390/ijms19061619

[60] L.C. Zhang, H. Attar, M. Calin, J. Eckert, Review on manufacture by selective laser melting and properties of titanium based materials for biomedical applications, Mater. Technol. 31 (2016) 66–76, https://doi.org/10.1179/1753555715Y.0000000076

[61] Y. Lv, Z. Ding, J. Xue, G. Sha, E. Lu, L. Wang, W. Lu, C. Su, L.-C. Zhang, Deformation mechanisms in surface nano-crystallization of low elastic modulus Ti6Al4V/Zn composite during severe plastic deformation, Scr. Mater. 157 (2018) 142–147, https://doi.org/10.1016/j.scriptamat.2018.08.007

[62] K. Kadirgama, W. Harun, F. Tarlochan, M. Samykano, D. Ramasamy, M.Z. Azir, H. Mehboob, Statistical and optimize of lattice structures with selective laser melting (SLM) of Ti6AL4V material, Int. J. Adv. Manuf. Technol. 97 (2018) 495–510, https://doi.org/10.1007/s00170-018-1913-1

[63] L.-C. Zhang, L.-Y. Chen, L. Wang, Surface modification of titanium and titanium alloys: technologies, developments, and future interests, Adv. Eng. Mater. 22 (2020), https://doi.org/10.1002/adem.201901258

[64] S. Liu, Y.C. Shin, Additive manufacturing of Ti6Al4V alloy: a review, Mater. Des. 164 (2019), https://doi.org/10.1016/j.matdes.2018.107552 (107552-107552).

[65] Kaur, Ghadirinejad, Oskouei, An overview on the tribological performance of titanium alloys with surface modifications for biomedical applications, Lubricants 7 (2019), https://doi.org/10.3390/lubricants7080065

[66] S.Y. Chen, J.C. Huang, C.T. Pan, C.H. Lin, T.L. Yang, Y.S. Huang, C.H. Ou, L.Y. Chen, D.Y. Lin, H.K. Lin, T.H. Li, J.S.C. Jang, C.C. Yang, Microstructure and mechanical properties of open-cell porous Ti-6Al-4V fabricated by selective laser melting, J. Alloy. Compd. 713 (2017) 248–254, https://doi.org/10.1016/j.jallcom.2017.04.190

[67] M. Fousová, D. Vojtěch, J. Kubásek, E. Jablonská, J. Fojt, Promising characteristics of gradient porosity Ti-6Al-4V alloy prepared by SLM process, J. Mech. Behav. Biomed. Mater. 69 (2017) 368–376, https://doi.org/10.1016/j.jmbbm.2017.01.043

[68] Y. Xu, D. Zhang, Y. Zhou, W. Wang, X. Cao, Study on topology optimization design, manufacturability, and performance evaluation of Ti-6Al-4V porous structures fabricated by selective laser melting (SLM), Materials 10 (2017), https://doi.org/10.3390/ma10091048

[69] N. Soro, H. Attar, X. Wu, M.S. Dargusch, Investigation of the structure and mechanical properties of additively manufactured Ti-6Al-4V biomedical scaffolds designed with a Schwartz primitive unit-cell, Mater. Sci. Eng. A 745 (2019) 195–202, https://doi.org/10.1016/j.msea.2018.12.104

[70] A. Arjunan, M. Demetriou, A. Baroutaji, C. Wang, Mechanical performance of highly permeable laser melted Ti6Al4V bone scaffolds, J. Mech. Behav. Biomed. Mater. 102 (2020) 103517, https://doi.org/10.1016/j.jmbbm.2019.103517

[71] A. Falkowska, A. Seweryn, M. Skrodzki, Strength properties of a porous titanium alloy Ti6Al4V with diamond structure obtained by laser power bed fusion (LPBF), Materials 13 (2020), https://doi.org/10.3390/ma13225138

[72] M.-W. Wu, J.-K. Chen, B.-H. Lin, P.-H. Chiang, M.-K. Tsai, Compressive fatigue properties of additive-manufactured Ti-6Al-4V cellular material with different porosities, Mater. Sci. Eng. A 790 (2020), https://doi.org/10.1016/j.msea.2020.139695

[73] F. Bartolomeu, M. Sampaio, O. Carvalho, E. Pinto, N. Alves, J.R. Gomes, F.S. Silva, G. Miranda, Tribological behavior of Ti6Al4V cellular structures produced by

selective laser melting, J. Mech. Behav. Biomed. Mater. 69 (2017) 128–134, https://doi.org/10.1016/j.jmbbm.2017.01.004
[74] L.X. Meng, D.D. Ben, H.J. Yang, H.B. Ji, D.L. Lian, Y.K. Zhu, J. Chen, J.L. Yi, L. Wang, J.B. Yang, Z.F. Zhang, Effects of embedded spherical pore on the tensile properties of a selective laser melted Ti6Al4V alloy, Mater. Sci. Eng. A 815 (2021), https://doi.org/10.1016/j.msea.2021.141254
[75] P. Didier, B. Piotrowski, M. Fischer, P. Laheurte, Mechanical stability of custom-made implants: Numerical study of anatomical device and low elastic Young's modulus alloy, Mater. Sci. Eng. C. Mater. Biol. Appl. 74 (2017) 399–409, https://doi.org/10.1016/j.msec.2016.12.031
[76] L. Bai, J. Zhang, X. Chen, C. Yi, R. Chen, Z. Zhang, Configuration optimization design of Ti6Al4V lattice structure formed by SLM, Materials 11 (2018), https://doi.org/10.3390/ma11101856
[77] K. Kadirgama, W.S.W. Harun, F. Tarlochan, M. Samykano, D. Ramasamy, M.Z. Azir, H. Mehboob, Statistical and optimize of lattice structures with selective laser melting (SLM) of Ti6AL4V material, Int. J. Adv. Manuf. Technol. 97 (2018) 495–510, https://doi.org/10.1007/s00170-018-1913-1
[78] X.-Y. Zhang, G. Fang, L.-L. Xing, W. Liu, J. Zhou, Effect of porosity variation strategy on the performance of functionally graded Ti-6Al-4V scaffolds for bone tissue engineering, Mater. Des. 157 (2018) 523–538, https://doi.org/10.1016/j.matdes.2018.07.064
[79] W.M. Peng, Y.F. Liu, X.F. Jiang, X.T. Dong, J. Jun, D.A. Baur, J.J. Xu, H. Pan, X. Xu, Bionic mechanical design and 3D printing of novel porous Ti6Al4V implants for biomedical applications, J. Zhejiang Univ. Sci. B 20 (2019) 647–659, https://doi.org/10.1631/jzus.B1800622
[80] J. Ge, J. Huang, Y. Lei, P. O'Reilly, M. Ahmed, C. Zhang, X. Yan, S. Yin, Microstructural features and compressive properties of SLM Ti6Al4V lattice structures, Surf. Coat. Technol. 403 (2020), https://doi.org/10.1016/j.surfcoat.2020.126419
[81] F. Bartolomeu, M.M. Costa, N. Alves, G. Miranda, F.S. Silva, Selective Laser Melting of Ti6Al4V sub-millimetric cellular structures: Prediction of dimensional deviations and mechanical performance, J. Mech. Behav. Biomed. Mater. 113 (2021) 104123, https://doi.org/10.1016/j.jmbbm.2020.104123
[82] H. Ali, L. Ma, H. Ghadbeigi, K. Mumtaz, In-situ residual stress reduction, martensitic decomposition and mechanical properties enhancement through high temperature powder bed pre-heating of selective laser melted Ti6Al4V, Mater. Sci. Eng. A 695 (2017) 211–220, https://doi.org/10.1016/j.msea.2017.04.033
[83] A.M. Khorasani, I. Gibson, A. Ghaderi, M.I. Mohammed, Investigation on the effect of heat treatment and process parameters on the tensile behaviour of SLM Ti-6Al-4V parts, Int. J. Adv. Manuf. Technol. 101 (2018) 3183–3197, https://doi.org/10.1007/s00170-018-3162-8
[84] M. Zhang, Y. Yang, D. Wang, Z. Xiao, C. Song, C. Weng, Effect of heat treatment on the microstructure and mechanical properties of Ti6Al4V gradient structures manufactured by selective laser melting, Mater. Sci. Eng. A 736 (2018) 288–297, https://doi.org/10.1016/j.msea.2018.08.084
[85] X. Yan, S. Yin, C. Chen, C. Huang, R. Bolot, R. Lupoi, M. Kuang, W. Ma, C. Coddet, H. Liao, M. Liu, Effect of heat treatment on the phase transformation and mechanical properties of Ti6Al4V fabricated by selective laser melting, J. Alloy. Compd. 764 (2018) 1056–1071, https://doi.org/10.1016/j.jallcom.2018.06.076
[86] X.-Y. Zhang, G. Fang, S. Leeflang, A.J. Böttger, A.A. Zadpoor, J. Zhou, Effect of subtransus heat treatment on the microstructure and mechanical properties of additively manufactured Ti-6Al-4V alloy, J. Alloy. Compd. 735 (2018) 1562–1575, https://doi.org/10.1016/j.jallcom.2017.11.263
[87] N. Jin, Z. Yan, Y. Wang, H. Cheng, H. Zhang, Effects of heat treatment on microstructure and mechanical properties of selective laser melted Ti-6Al-4V lattice materials, Int. J. Mech. 190 (2021), https://doi.org/10.1016/j.ijmecsci.2020.106042
[88] M.-W. Wu, J.-K. Chen, B.-H. Lin, P.-H. Chiang, Improved fatigue endurance ratio of additive manufactured Ti-6Al-4V lattice by hot isostatic pressing, Mater. Des. 134 (2017) 163–170, https://doi.org/10.1016/j.matdes.2017.08.048
[89] B. Zhou, J. Zhou, H. Li, F. Lin, A study of the microstructures and mechanical properties of Ti6Al4V fabricated by SLM under vacuum, Mater. Sci. Eng. A 724 (2018) 1–10, https://doi.org/10.1016/j.msea.2018.03.021
[90] C. Chen, Y. Xie, X. Yan, S. Yin, H. Fukanuma, R. Huang, R. Zhao, J. Wang, Z. Ren, M. Liu, H. Liao, Effect of hot isostatic pressing (HIP) on microstructure and mechanical properties of Ti6Al4V alloy fabricated by cold spray additive manufacturing, Addit. Manuf. 27 (2019) 595–605, https://doi.org/10.1016/j.addma.2019.03.028
[91] H. Yu, F. Li, Z. Wang, X. Zeng, Fatigue performances of selective laser melted Ti-6Al-4V alloy: influence of surface finishing, hot isostatic pressing and heat treatments, Int. J. Fatigue 120 (2019) 175–183, https://doi.org/10.1016/j.ijfatigue.2018.11.019
[92] J. Li, Z. Li, R. Li, Y. Shi, H. Wang, Y. Wang, G. Jin, In vitro and in vivo evaluations of mechanical properties, biocompatibility and osteogenic ability of sintered porous titanium alloy implant, RSC Adv. 8 (2018) 36512–36520, https://doi.org/10.1039/c8ra07518b
[93] S.I. Stepanov, Y.N. Loginov, V.P. Kuznetsov, A.A. Popov, Effect of annealing on the structure and properties of titanium alloy with cellular architecture for medical applications, Met. Sci. Heat. Treat. 60 (2018) 315–321, https://doi.org/10.1007/s11041-018-0278-2
[94] N. Taniguchi, S. Fujibayashi, M. Takemoto, K. Sasaki, B. Otsuki, T. Nakamura, T. Matsushita, T. Kokubo, S. Matsuda, Effect of pore size on bone ingrowth into porous titanium implants fabricated by additive manufacturing: an in vivo experiment, Mater. Sci. Eng. C Mater. Biol. Appl. 59 (2016) 690–701, https://doi.org/10.1016/j.msec.2015.10.069
[95] H. Pereira, I.F. Cengiz, F.R. Maia, F. Bartolomeu, J.M. Oliveira, R.L. Reis, F.S. Silva, Physicochemical properties and cytocompatibility assessment of non-degradable scaffolds for bone tissue engineering applications, J. Mech. Behav. Biomed. Mater. 112 (2020) 103997, https://doi.org/10.1016/j.jmbbm.2020.103997
[96] J. Tang, R. Peng, J. Ding, The regulation of stem cell differentiation by cell-cell contact on micropatterned material surfaces, Biomaterials 31 (2010) 2470–2476, https://doi.org/10.1016/j.biomaterials.2009.12.006
[97] B.K. Nagesha, V. Dhinakaran, M. Varsha Shree, K.P. Manoj Kumar, D. Chalawadi, T. Sathish, Review on characterization and impacts of the lattice structure in additive manufacturing, Mater. Today. Proc. 21 (2020) 916–919, https://doi.org/10.1016/j.matpr.2019.08.158
[98] F. Liu, Z. Mao, P. Zhang, D.Z. Zhang, J. Jiang, Z. Ma, Functionally graded porous scaffolds in multiple patterns: new design method, physical and mechanical properties, Mater. Des. 160 (2018) 849–860, https://doi.org/10.1016/j.matdes.2018.09.053
[99] J. Maszybrocka, B. Gapiński, M. Dworak, G. Skrabalak, A. Stwora, The manufacturability and compression properties of the Schwarz Diamond type Ti6Al4V cellular lattice fabricated by selective laser melting, Int. J. Adv. Manuf. Technol. 105 (2019) 3411–3425, https://doi.org/10.1007/s00170-019-04422-6
[100] X. Pei, B. Zhang, Y. Fan, X. Zhu, Y. Sun, Q. Wang, X. Zhang, C. Zhou, Bionic mechanical design of titanium bone tissue implants and 3D printing manufacture, Mater. Lett. 208 (2017) 133–137, https://doi.org/10.1016/j.matlet.2017.04.128
[101] H.A. Zaharin, A.M. Abdul Rani, F.I. Azam, T.L. Ginta, N. Sallih, A. Ahmad, N.A. Yunus, T.Z.A. Zulkifli, Effect of unit cell type and pore size on porosity and mechanical behavior of additively manufactured Ti6Al4V scaffolds, Materials 11 (2018), https://doi.org/10.3390/ma11122402
[102] Y. Li, C. Yang, H. Zhao, S. Qu, X. Li, Y. Li, New developments of Ti-based alloys for biomedical applications, Materials 7 (2014) 1709–1800, https://doi.org/10.3390/ma7031709
[103] L. Li, J. Shi, K. Zhang, L. Yang, F. Yu, L. Zhu, H. Liang, X. Wang, Q. Jiang, Early osteointegration evaluation of porous Ti6Al4V scaffolds designed based on triply periodic minimal surface models, J. Orthop. Transl. 19 (2019) 94–105, https://doi.org/10.1016/j.jot.2019.03.003
[104] J. Li, W. Li, Z. Li, Y. Wang, R. Li, J. Tu, G. Jin, In vitro and in vivo evaluations of the fully porous Ti6Al4V acetabular cups fabricated by a sintering technique, RSC Adv. 9 (2019) 6724–6732, https://doi.org/10.1039/c9ra00638a
[105] V.S. Cheong, P. Fromme, M.J. Coathup, A. Mumith, G.W. Blunn, Partial bone formation in additive manufactured porous implants reduces predicted stress and danger of fatigue failure, Ann. Biomed. Eng. 48 (2020) 502–514, https://doi.org/10.1007/s10439-019-02369-z
[106] L.Y. Chen, J.C. Huang, C.H. Lin, C.T. Pan, S.Y. Chen, T.L. Yang, D.Y. Lin, H.K. Lin, J.S.C. Jang, Anisotropic response of Ti-6Al-4V alloy fabricated by 3D printing selective laser melting, Mater. Sci. Eng. A 682 (2017) 389–395, https://doi.org/10.1016/j.msea.2016.11.061
[107] J.Y. Cho, W. Xu, M. Brandt, M. Qian, Selective laser melting-fabricated Ti-6Al-4V alloy: microstructural inhomogeneity, consequent variations in elastic modulus and implications, Opt. Laser Technol. 111 (2019) 664–670, https://doi.org/10.1016/j.optlastec.2018.08.052
[108] M. Elsayed, M. Ghazy, Y. Youssef, K. Essa, Optimization of SLM process parameters for Ti6Al4V medical implants, Rapid Prototyp. J. 25 (2019) 433–447, https://doi.org/10.1108/rpj-05-2018-0112
[109] B. Vayssette, N. Saintier, C. Brugger, M. El May, Surface roughness effect of SLM and EBM Ti-6Al-4V on multiaxial high cycle fatigue, Theor. Appl. Fract. Mech. 108 (2020) 102581, https://doi.org/10.1016/j.tafmec.2020.102581
[110] J. Li, X. Cui, G.J. Hooper, K.S. Lim, T.B.F. Woodfield, Rational design, bio-functionalization and biological performance of hybrid additive manufactured titanium implants for orthopaedic applications: a review, J. Mech. Behav. Biomed. Mater. 105 (2020) 103671, https://doi.org/10.1016/j.jmbbm.2020.103671
[111] X. Zhao, S. Li, M. Zhang, Y. Liu, T.B. Sercombe, S. Wang, Y. Hao, R. Yang, L.E. Murr, Comparison of the microstructures and mechanical properties of Ti-6Al-4V fabricated by selective laser melting and electron beam melting, Mater. Des. 95 (2016) 21–31, https://doi.org/10.1016/j.matdes.2015.12.135
[112] W. Xu, E.W. Lui, A. Pateras, M. Qian, M. Brandt, In situ tailoring microstructure in additively manufactured Ti-6Al-4V for superior mechanical performance, Acta Mater. 125 (2017) 390–400, https://doi.org/10.1016/j.actamat.2016.12.027
[113] J. Mutua, S. Nakata, T. Onda, Z.-c Chen, Optimization of selective laser melting parameters and in fl uence of post heat treatment on microstructure and mechanical properties of maraging steel, Mater. Des. 139 (2018) 486–497, https://doi.org/10.1016/j.matdes.2017.11.042
[114] A.H. Maamoun, Y.F. Xue, M.A. Elbestawi, S.C. Veldhuis, Effect of selective laser melting process parameters on the quality of Al alloy parts: powder characterization, density, surface roughness, and dimensional accuracy, Materials 11 (2018), https://doi.org/10.3390/ma11122343
[115] M.F. Sadali, Effect of hatching distance on surface morphology and surface roughness of the Ti6Al4V for biomedical implant using SLM process, Malays. J. Microsc. 15 (2019) 72–82.
[116] B. Song, S. Dong, B. Zhang, H. Liao, C. Coddet, Effects of processing parameters on microstructure and mechanical property of selective laser melted Ti6Al4V, Mater. Des. 35 (2012) 120–125, https://doi.org/10.1016/j.matdes.2011.09.051
[117] W. Xiong, L. Hao, Y. Li, D. Tang, Q. Cui, Z. Feng, C. Yan, Effect of selective laser melting parameters on morphology, microstructure, densi fi cation and mechanical properties of supersaturated silver alloy, Mater. Des. 170 (2019), https://doi.org/10.1016/j.matdes.2019.107697

[118] W. Liu, S. Liu, L. Wang, Surface modification of biomedical titanium alloy: micromorphology, microstructure evolution and biomedical applications, Coatings 9 (2019), https://doi.org/10.3390/coatings9040249
[119] A. Jemat, M.J. Ghazali, M. Razali, Y. Otsuka, Surface modifications and their effects on titanium dental implants, Biomed. Res. Int. 2015 (2015), https://doi.org/10.1155/2015/791725
[120] B. Vayssette, N. Saintier, C. Brugger, M. Elmay, E. Pessard, Surface roughness of Ti-6Al-4V parts obtained by SLM and EBM: effect on the high cycle fatigue life, Procedia Eng. 213 (2018) 89–97, https://doi.org/10.1016/j.proeng.2018.02.010
[121] P. Ginestra, R.M. Ferraro, K. Zohar-Hauber, A. Abeni, S. Giliani, E. Ceretti, Selective laser melting and electron beam melting of Ti6Al4V for orthopedic applications: a comparative study on the applied building direction, Materials 13 (2020), https://doi.org/10.3390/ma13235584
[122] V. Goriainov, R. Cook, J.M. Latham, D.G. Dunlop, R.O.C. Oreffo, Bone and metal: an orthopaedic perspective on osseointegration of metals, Acta Biomater. 10 (2014) 4043–4057, https://doi.org/10.1016/j.actbio.2014.06.004
[123] N. Singh, P. Hameed, R. Ummethala, G. Manivasagam, K.G. Prashanth, Selective laser manufacturing of Ti-based alloys and composites: impact of process parameters, application trends, and future prospects, Mater. Today Adv. 8 (2020), https://doi.org/10.1016/j.mtadv.2020.100097 (100097-100097).
[124] M. de Wild, R. Schumacher, K. Mayer, E. Schkommodau, D. Thoma, M. Bredell, A. Kruse Gujer, K.W. Gratz, F.E. Weber, Bone regeneration by the osteoconductivity of porous titanium implants manufactured by selective laser melting: a histological and micro computed tomography study in the rabbit, Tissue Eng. Part A 19 (2013) 2645–2654, https://doi.org/10.1089/ten.TEA.2012.0753
[125] J.Y. Xu, X.S. Chen, C.Y. Zhang, Y. Liu, J. Wang, F.L. Deng, Improved bioactivity of selective laser melting titanium: surface modification with micro-/nano-textured hierarchical topography and bone regeneration performance evaluation, Mater. Sci. Eng. C Mater. Biol. Appl. 68 (2016) 229–240, https://doi.org/10.1016/j.msec.2016.05.096
[126] S. Van Bael, Y.C. Chai, S. Truscello, M. Moesen, G. Kerckhofs, H. Van Oosterwyck, J.P. Kruth, J. Schrooten, The effect of pore geometry on the in vitro biological behavior of human periosteum-derived cells seeded on selective laser-melted Ti6Al4V bone scaffolds, Acta Biomater. 8 (2012) 2824–2834, https://doi.org/10.1016/j.actbio.2012.04.001
[127] B. Wysocki, J. Idaszek, K. Szlazak, K. Strzelczyk, T. Brynk, K.J. Kurzydlowski, W. Swieszkowski, Post processing and biological evaluation of the titanium scaffolds for bone tissue engineering, Materials 9 (2016), https://doi.org/10.3390/ma9030197
[128] M. Wang, T. Chen, S. Lu, Y. Zhao, H. Chen, Y. Wu, Z. Tang, Osteogenic comparison on selective laser melting printed and sandblasting-acid-etching Ti substrates for customized implant applications, Sci. Adv. Mater. 9 (2017) 705–714, https://doi.org/10.1166/sam.2017.3012
[129] A. Balyakin, E. Zhuchenko, E. Nosova, Study of heat treatment impact on the surface defects appearance on samples obtained by selective laser melting of Ti-6Al-4V during chemical polishing, Mater. Today. Proc. 19 (2019) 2307–2311, https://doi.org/10.1016/j.matpr.2019.07.676
[130] T. Thenard, A. Catapano, R. Allena, M. El May, N. Saintier, M. Mesnard, Topography and wettability characterization of surfaces manufactured by SLM and treated by chemical etching, Mech. Adv. Mater. Struct. (2020) 1–18, https://doi.org/10.1080/15376494.2020.1836292
[131] B. Vayssette, N. Saintier, C. Brugger, M. El May, Surface roughness effect of SLM and EBM Ti-6Al-4V on multiaxial high cycle fatigue, Theor. Appl. Fract. Mech. 108 (2020), https://doi.org/10.1016/j.tafmec.2020.102581
[132] J. Günther, S. Leuders, P. Koppa, T. Tröster, S. Henkel, H. Biermann, T. Niendorf, On the effect of internal channels and surface roughness on the high-cycle fatigue performance of Ti-6Al-4V processed by SLM, Mater. Des. 143 (2018) 1–11, https://doi.org/10.1016/j.matdes.2018.01.042
[133] V. Chastand, A. Tezenas, Y. Cadoret, P. Quaegebeur, W. Maia, E. Charkaluk, Fatigue characterization of Titanium Ti-6Al-4V samples produced by additive manufacturing, Procedia Struct. Integr. 2 (2016) 3168–3176, https://doi.org/10.1016/j.prostr.2016.06.395
[134] J.E. González, Gd Armas, J. Negrin, A.M. Beltrán, P. Trueba, F.J. Gotor, E. Peón, Y. Torres, Influence of successive chemical and thermochemical treatments on surface features of Ti6Al4V samples manufactured by SLM, Metals 11 (2021), https://doi.org/10.3390/met11020313
[135] P.T.M. Le, S.A. Shintani, H. Takadama, M. Ito, T. Kakutani, H. Kitagaki, S. Terauchi, T. Ueno, H. Nakano, Y. Nakajima, K. Inoue, T. Matsushita, S. Yamaguchi, Bioactivation treatment with mixed acid and heat on titanium implants fabricated by selective laser melting enhances preosteoblast cell differentiation, Nanomaterials 11 (2021), https://doi.org/10.3390/nano11040987
[136] A. Fukuda, M. Takemoto, T. Saito, S. Fujibayashi, M. Neo, D.K. Pattanayak, T. Matsushita, K. Sasaki, N. Nishida, T. Kokubo, T. Nakamura, Osteoinduction of porous Ti implants with a channel structure fabricated by selective laser melting, Acta Biomater. 7 (2011) 2327–2336, https://doi.org/10.1016/j.actbio.2011.01.037
[137] D.K. Pattanayak, A. Fukuda, T. Matsushita, M. Takemoto, S. Fujibayashi, K. Sasaki, N. Nishida, T. Nakamura, T. Kokubo, Bioactive Ti metal analogous to human cancellous bone: fabrication by selective laser melting and chemical treatments, Acta Biomater. 7 (2011) 1398–1406, https://doi.org/10.1016/j.actbio.2010.09.034
[138] S. Amin Yavari, J. van der Stok, Y.C. Chai, R. Wauthle, Z. Tahmasebi Birgani, P. Habibovic, M. Mulier, J. Schrooten, H. Weinans, A.A. Zadpoor, Bone regeneration performance of surface-treated porous titanium, Biomaterials 35 (2014) 6172–6181, https://doi.org/10.1016/j.biomaterials.2014.04.054
[139] M. Tsukanaka, S. Fujibayashi, M. Takemoto, T. Matsushita, T. Kokubo, T. Nakamura, K. Sasaki, S. Matsuda, Bioactive treatment promotes osteoblast differentiation on titanium materials fabricated by selective laser melting technology, Dent. Mater. J. 35 (2016) 118–125, https://doi.org/10.4012/dmj.2015-127
[140] C.I.f.H. Information, Hip and Knee Replacements in Canada, 2018–2019 (2020)
[141] E.A. Masters, R.P. Trombetta, K.L. de Mesy Bentley, B.F. Boyce, A.L. Gill, S.R. Gill, K. Nishitani, M. Ishikawa, Y. Morita, H. Ito, Evolving concepts in bone infection: redefining “biofilm”,“acute vs. chronic osteomyelitis”,“the immune proteome” and “local antibiotic therapy”, Bone Res. 7 (2019) 1–18, https://doi.org/10.1038/s41413-019-0061-z
[142] S.K. Schmitt, Osteomyelitis, Infect. Dis. Clin. North Am. 31 (2017) 325–338, https://doi.org/10.1016/j.idc.2017.01.010
[143] K.P. Rumbaugh, K. Sauer, Biofilm dispersion, Nat. Rev. Microbiol 18 (2020) 571–586, https://doi.org/10.1038/s41579-020-0385-0
[144] N.J. Hickok, I.M. Shapiro, Immobilized antibiotics to prevent orthopaedic implant infections, Adv. Drug Deliv. Rev. 64 (2012) 1165–1176, https://doi.org/10.1016/j.addr.2012.03.015
[145] A. Besinis, S.D. Hadi, H.R. Le, C. Tredwin, R.D. Handy, Antibacterial activity and biofilm inhibition by surface modified titanium alloy medical implants following application of silver, titanium dioxide and hydroxyapatite nanocoatings, Nanotoxicology 11 (2017) 327–338, https://doi.org/10.1080/17435390.2017.1299890
[146] I.A.J. van Hengel, M. Riool, L.E. Fratila-Apachitei, J. Witte-Bouma, E. Farrell, A.A. Zadpoor, S.A.J. Zaat, I. Apachitei, Selective laser melting porous metallic implants with immobilized silver nanoparticles kill and prevent biofilm formation by methicillin-resistant Staphylococcus aureus, Biomaterials 140 (2017) 1–15, https://doi.org/10.1016/j.biomaterials.2017.02.030
[147] M. Fazel, H.R. Salimijazi, M. Shamanian, M. Minneboo, K. Modaresifar, I.A.J. van Hengel, L.E. Fratila-Apachitei, I. Apachitei, A.A. Zadpoor, Osteogenic and antibacterial surfaces on additively manufactured porous Ti-6Al-4V implants: combining silver nanoparticles with hydrothermally synthesized HA nanocrystals, Mater. Sci. Eng. C Mater. Biol. Appl. 120 (2021) 111745, https://doi.org/10.1016/j.msec.2020.111745
[148] A. Shivaram, S. Bose, A. Bandyopadhyay, Understanding long-term silver release from surface modified porous titanium implants, Acta Biomater. 58 (2017) 550–560, https://doi.org/10.1016/j.actbio.2017.05.048
[149] G. Zhang, P. Zhao, L. Lin, L. Qin, Z. Huan, S. Leeflang, A.A. Zadpoor, J. Zhou, L. Wu, Surface-treated 3D printed Ti-6Al-4V scaffolds with enhanced bone regeneration performance: an in vivo study, Ann. Transl. Med. 9 (2021) 39, https://doi.org/10.21037/atm-20-3829
[150] X. Ye, S. Leeflang, C. Wu, J. Chang, J. Zhou, Z. Huan, Mesoporous bioactive glass functionalized 3D Ti-6Al-4V scaffolds with improved surface bioactivity, Materials 10 (2017), https://doi.org/10.3390/ma10111244
[151] W.H. Kao, Y.L. Su, J.H. Horng, C.Y. Chang, Tribological, electrochemical and biocompatibility properties of Ti6Al4V alloy produced by selective laser melting method and then processed using gas nitriding, CN or Ti-C:H coating treatments, Surf. Coat. Technol. 350 (2018) 172–187, https://doi.org/10.1016/j.surfcoat.2018.07.011
[152] X. Zhao, H. Zhang, H. Liu, S. Li, W. Li, X. Wang, In vitro bio-tribological behaviour of textured nitride coating on selective laser melted Ti-6Al-4V alloy, Surf. Coat. Technol. 409 (2021), https://doi.org/10.1016/j.surfcoat.2021.126904
[153] C. Yan, L. Hao, A. Hussein, Q. Wei, Y. Shi, Microstructural and surface modifications and hydroxyapatite coating of Ti-6Al-4V triply periodic minimal surface lattices fabricated by selective laser melting, Mater. Sci. Eng. C Mater. Biol. Appl. 75 (2017) 1515–1524, https://doi.org/10.1016/j.msec.2017.03.066
[154] G.-F. Zhang, X. Liu, S. Zhang, B. Pan, M.-L. Liu, Ciprofloxacin derivatives and their antibacterial activities, Eur. J. Med. Chem. 146 (2018) 599–612, https://doi.org/10.1016/j.ejmech.2018.01.078
[155] C.A. Igwegbe, S.N. Oba, C.O. Aniagor, A.G. Adeniyi, J.O. Ighalo, Adsorption of ciprofloxacin from water: a comprehensive review, J. Ind. Eng. Chem. J. (2020), https://doi.org/10.1016/j.jiec.2020.09.023
[156] J. Vaithilingam, S. Kilsby, R.D. Goodridge, S.D.R. Christie, S. Edmondson, R.J.M. Hague, Immobilisation of an antibacterial drug to Ti6Al4V components fabricated using selective laser melting, Appl. Surf. Sci. 314 (2014) 642–654, https://doi.org/10.1016/j.apsusc.2014.06.014
[157] G. Wang, W. Jin, A.M. Qasim, A. Gao, X. Peng, W. Li, H. Feng, P.K. Chu, Antibacterial effects of titanium embedded with silver nanoparticles based on electron-transfer-induced reactive oxygen species, Biomaterials 124 (2017) 25–34, https://doi.org/10.1016/j.biomaterials.2017.01.028
[158] M. Godoy-Gallardo, A.G. Rodriguez-Hernandez, L.M. Delgado, J.M. Manero, F. Javier Gil, D. Rodriguez, Silver deposition on titanium surface by electrochemical anodizing process reduces bacterial adhesion of Streptococcus sanguinis and Lactobacillus salivarius, Clin. Oral. Implants Res. 26 (2015) 1170–1179, https://doi.org/10.1111/clr.12422
[159] N. Dai, L.-C. Zhang, J. Zhang, Q. Chen, M. Wu, Corrosion behavior of selective laser melted Ti-6Al-4 V alloy in NaCl solution, Corros. Sci. 102 (2016) 484–489, https://doi.org/10.1016/j.corsci.2015.10.041
[160] N. Dai, J. Zhang, Y. Chen, L.-C. Zhang, Heat treatment degrading the corrosion resistance of selective laser melted Ti-6Al-4V alloy, J. Electrochem. Soc. 164 (2017) C428–C434, https://doi.org/10.1149/2.1481707jes
[161] A. Sharma, M.C. Oh, J.-T. Kim, A.K. Srivastava, B. Ahn, Investigation of electrochemical corrosion behavior of additive manufactured Ti–6Al–4V alloy for medical implants in different electrolytes, J. Alloy. Compd. 830 (2020), https://doi.org/10.1016/j.jallcom.2020.154620

[162] G. Chi, D. Yi, H. Liu, Effect of roughness on electrochemical and pitting corrosion of Ti-6Al-4V alloy in 12 wt% HCl solution at 35 °C, J. Mater. Res. Technol. 9 (2020) 1162–1174, https://doi.org/10.1016/j.jmrt.2019.11.044
[163] G.K. Schwalfenberg, The alkaline diet: is there evidence that an alkaline pH diet benefits health? J. Environ. Public Health 2012 (2012), https://doi.org/10.1155/2012/727630 (727630-727630).
[164] X. Yan, C. Shi, T. Liu, Y. Ye, C. Chang, W. Ma, C. Deng, S. Yin, H. Liao, M. Liu, Effect of heat treatment on the corrosion resistance behavior of selective laser melted Ti6Al4V ELI, Surf. Coat. Technol. 396 (2020), https://doi.org/10.1016/j.surfcoat.2020.125955
[165] S. Pal, M. Finšgar, T. Bončina, G. Lojen, T. Brajlih, I. Drstvenšek, Effect of surface powder particles and morphologies on corrosion of Ti-6Al-4 V fabricated with different energy densities in selective laser melting, Mater. Des. 211 (2021), https://doi.org/10.1016/j.matdes.2021.110184
[166] G.A. Longhitano, M.A. Arenas, A. Conde, M.A. Larosa, A.L. Jardini, C.Ad.C. Zavaglia, J.J. Damborenea, Heat treatments effects on functionalization and corrosion behavior of Ti-6Al-4V ELI alloy made by additive manufacturing, J. Alloy. Compd. 765 (2018) 961–968, https://doi.org/10.1016/j.jallcom.2018.06.319
[167] H. Zhang, C. Man, C. Dong, L. Wang, W. Li, D. Kong, L. Wang, X. Wang, The corrosion behavior of Ti6Al4V fabricated by selective laser melting in the artificial saliva with different fluoride concentrations and pH values, Corros. Sci. 179 (2021), https://doi.org/10.1016/j.corsci.2020.109097
[168] P. Qin, L.Y. Chen, Y.J. Liu, Z. Jia, S.X. Liang, C.H. Zhao, H. Sun, L.C. Zhang, Corrosion and passivation behavior of laser powder bed fusion produced Ti-6Al-4V in static/dynamic NaCl solutions with different concentrations, Corros. Sci. 191 (2021), https://doi.org/10.1016/j.corsci.2021.109728
[169] Q. Zhang, B. Duan, Z. Zhang, J. Wang, C. Si, Effect of ultrasonic shot peening on microstructure evolution and corrosion resistance of selective laser melted Ti–6Al–4V alloy, J. Mater. Res. Technol. 11 (2021) 1090–1099, https://doi.org/10.1016/j.jmrt.2021.01.091
[170] H. Lu, Z. Wang, J. Cai, X. Xu, K. Luo, L. Wu, J. Lu, Effects of laser shock peening on the hot corrosion behaviour of the selective laser melted Ti6Al4V titanium alloy, Corros. Sci. 188 (2021), https://doi.org/10.1016/j.corsci.2021.109558
[171] J.P.L. do Nascimento, M.O.A. Ferreira, R.V. Gelamo, J. Scarmínio, T.T. Steffen, B.P. da Silva, I.V. Aoki, A.G. dos Santos Jr, V.V. de Castro, C. de Fraga Malfatti, J.A. Moreto, Enhancing the corrosion protection of Ti-6Al-4V alloy through reactive sputtering niobium oxide thin films, Surf. Coat. Technol. 428 (2021) 127854, https://doi.org/10.1016/j.surfcoat.2021.127854
[172] P. Lei, H. Qian, T. Zhang, T. Lei, Y. Hu, C. Chen, K. Zhou, Porous tantalum structure integrated on Ti6Al4V base by laser powder bed fusion for enhanced bony-ingrowth implants: in vitro and in vivo validation, Bioact. Mater. 7 (2022) 3–13.
[173] Q. Sui, L. Meng, S. Wang, P. Li, X. Yin, L. Wang, Effect of Nb addition on mechanical properties and corrosion behavior of Ti6Al4V alloy produced by selective laser melting, J. Mater. Res. 35 (2020) 571–579, https://doi.org/10.1557/jmr.2019.415
[174] Q. Wang, C. Han, T. Choma, Q. Wei, C. Yan, B. Song, Y. Shi, Effect of Nb content on microstructure, property and in vitro apatite-forming capability of Ti-Nb alloys fabricated via selective laser melting, Mater. Des. 126 (2017) 268–277, https://doi.org/10.1016/j.matdes.2017.04.026
[175] S.L. Sing, F.E. Wiria, W.Y. Yeong, Selective laser melting of titanium alloy with 50 wt% tantalum: Effect of laser process parameters on part quality, Int. J. Refract. Met. Hard Mater. 77 (2018) 120–127, https://doi.org/10.1016/j.ijrmhm.2018.08.006
[176] S.L. Campanelli, N. Contuzzi, A.D. Ludovico, F. Caiazzo, F. Cardaropoli, V. Sergi, Manufacturing and characterization of Ti6Al4V lattice components manufactured by selective laser melting, Materials 7 (2014) 4803–4822, https://doi.org/10.3390/ma7064803
[177] A. Chuang, J. Erlebacher, Challenges and opportunities for integrating dealloying methods into additive manufacturing, Materials 13 (2020), https://doi.org/10.3390/ma13173706
[178] A. Chuang, J. Erlebacher, Challenges and opportunities for integrating dealloying methods into additive manufacturing, Materials 13 (2020) 3706.
[179] T. Song, M. Yan, M. Qian, The enabling role of dealloying in the creation of specific hierarchical porous metal structures – a review, Corros. Sci. 134 (2018) 78–98, https://doi.org/10.1016/j.corsci.2018.02.013
[180] C. Yang, C. Zhang, L. Liu, Excellent degradation performance of 3D hierarchical nanoporous structures of copper towards organic pollutants, J. Mater. Chem. A 6 (2018) 20992–21002, https://doi.org/10.1039/C8TA07973K
[181] Y.-H. Li, X.-Y. Shang, Recent progress in porous TiNb-based alloys for biomedical implant applications, Mater. Sci. Technol. 36 (2020) 385–392, https://doi.org/10.1080/02670836.2020.1724415
[182] Y. Luo, Y. Jiang, J. Zhu, J. Tu, S. Jiao, Surface treatment functionalization of sodium hydroxide onto 3D printed porous Ti6Al4V for improved biological activities and osteogenic potencies, J. Mater. Res. Technol. 9 (2020) 13661–13670, https://doi.org/10.1016/j.jmrt.2020.09.076
[183] S. Suresh, S. Chen-Nan, S. Tekumalla, V. Rosa, S.M.L. Nai, R. Wong, Mechanical properties and in vitro cytocompatibility of dense and porous Ti–6Al–4V ELI manufactured by selective laser melting technology for biomedical applications, J. Mech. Behav. Biomed. Mater. (2021) 104712, https://doi.org/10.1016/j.jmbbm.2021.104712
[184] E. De Giglio, D. Cafagna, S. Cometa, A. Allegretta, A. Pedico, L.C. Giannossa, L. Sabbatini, M. Mattioli-Belmonte, R. Iatta, An innovative, easily fabricated, silver nanoparticle-based titanium implant coating: development and analytical characterization, Anal. Bioanal. Chem. 405 (2013) 805–816, https://doi.org/10.1007/s00216-012-6293-z
[185] Z. Jia, P. Xiu, P. Xiong, W. Zhou, Y. Cheng, S. Wei, Y. Zheng, T. Xi, H. Cai, Z. Liu, C. Wang, W. Zhang, Z. Li, Additively manufactured macroporous titanium with silver-releasing micro-/nanoporous surface for multipurpose infection control and bone repair – a Proof of Concept, ACS Appl. Mater. Interfaces 8 (2016) 28495–28510, https://doi.org/10.1021/acsami.6b10473
[186] R.D.P. Reddy, V. Sharma, Additive manufacturing in drug delivery applications: a review, Int. J. Pharm. 589 (2020) 119820, https://doi.org/10.1016/j.ijpharm.2020.119820
[187] A. Takase, T. Ishimoto, R. Suganuma, T. Nakano, Lattice distortion in selective laser melting (SLM)-manufactured unstable β-type Ti-15Mo-5Zr-3Al alloy analyzed by high-precision X-ray diffractometry, Scr. Mater. 201 (2021) 113953, https://doi.org/10.1016/j.scriptamat.2021.113953
[188] K.M. D'Souza, M.A. Aras, Types of implant surgical guides in dentistry: a review, J. Oral. Implantol. 38 (2012) 643–652, https://doi.org/10.1563/AAID-JOI-D-11-00018
[189] D. Srinivasan, A. Singh, A.S. Reddy, K. Chatterjee, Microstructural study and mechanical characterisation of heat-treated direct metal laser sintered Ti6Al4V for biomedical applications, Mater. Technol. (2020) 1–12, https://doi.org/10.1080/10667857.2020.1830566
[190] M.C. Kayacan, Y.B. Baykal, T. Karaaslan, K. Özsoy, İ. Alaca, B. Duman, Y.E. Delikanlı, Monitoring the osseointegration process in porous Ti6Al4V implants produced by additive manufacturing: an experimental study in sheep, J. Appl. Biomater. Funct. Mater. 16 (2018) 68–75, https://doi.org/10.5301/jabfm.5000385
[191] D. Chioibasu, L. Duta, G. Popescu-Pelin, N. Popa, N. Milodin, S. Iosub, L.M. Balescu, A. Catalin Galca, A. Claudiu Popa, F.N. Oktar, Animal origin bioactive hydroxyapatite thin films synthesized by RF-magnetron sputtering on 3D printed cranial implants, Metals 9 (2019) 1332, https://doi.org/10.3390/met9121332
[192] J.C. Kennon, C. Lu, M.E. McGee-Lawrence, L.A. Crosby, Scapula fracture incidence in reverse total shoulder arthroplasty using screws above or below metaglene central cage: clinical and biomechanical outcomes, J. Shoulder Elb. Surg. 26 (2017) 1023–1030, https://doi.org/10.1016/j.jse.2016.10.018
[193] J.M. Tatro, J.P. Anderson, D.L. McCreary, L.K. Schroder, P.A. Cole, Radiographic correlation of clinical shoulder deformity and patient perception following scapula fracture, Injury 51 (2020) 1584–1591, https://doi.org/10.1016/j.injury.2020.04.017
[194] A. Postler, C. Lützner, F. Beyer, E. Tille, J. Lützner, Analysis of total knee arthroplasty revision causes, BMC Musculoskelet. Disord. 19 (2018) 1–6, https://doi.org/10.1186/s12891-018-1977-y
[195] N.A. Bedard, J.M. Elkins, T.S. Brown, Effect of COVID-19 on hip and knee arthroplasty surgical volume in the United States, J. Arthroplast. 35 (2020) S45–S48, https://doi.org/10.1016/j.arth.2020.04.060
[196] S.K. Kunutsor, M.C. Barrett, A.D. Beswick, A. Judge, A.W. Blom, V. Wylde, M.R. Whitehouse, Risk factors for dislocation after primary total hip replacement: a systematic review and meta-analysis of 125 studies involving approximately five million hip replacements, Lancet 1 (2019) e111–e121, https://doi.org/10.1016/S2665-9913(19)30045-1
[197] C. Rivière, J.-Y. Lazennec, C. Van Der Straeten, E. Auvinet, J. Cobb, S. Muirhead-Allwood, The influence of spine-hip relations on total hip replacement: a systematic review, OTSR 103 (2017) 559–568, https://doi.org/10.1016/j.otsr.2017.02.014
[198] C.P. DiPaola, R.W. Molinari, Posterior lumbar interbody fusion, J. Am. Acad. Orthop. Surg. J. Am. Acad. Orthop. SUR 16 (2008) 130–139, https://doi.org/10.5435/00124635-200803000-00004
[199] D.S. Xu, C.T. Walker, J. Godzik, J.D. Turner, W. Smith, J.S. Uribe, Minimally invasive anterior, lateral, and oblique lumbar interbody fusion: a literature review, Ann. Transl. Med. 6 (2018), https://doi.org/10.21037/atm.2018.03.24
[200] S.D. Castellanos, J.L. Alves, R.J. Neto, A comparative study of manufacturing processes of complex surface parts in Titanium Ti6Al4V, Ciência Tecnol. Dos. Mater. 29 (2017) 73–78, https://doi.org/10.1016/j.ctmat.2017.03.002
[201] G. Kitamura, M.B.V. Albers, B.P. Lesniak, S.J. Rabuck, V. Musahl, C.L. Andrews, A. Ghodadra, F. Fu, 3-dimensional printed models may be a useful tool when planning revision anterior cruciate ligament reconstruction, Arthrosc., Sports Med., Rehabil. 1 (2019) e41–e46, https://doi.org/10.1016/j.asmr.2019.06.004
[202] F. Deng, L. Liu, Z. Li, J. Liu, 3D printed Ti6Al4V bone scaffolds with different pore structure effects on bone ingrowth, J. Biol. Eng. 15 (2021) 4, https://doi.org/10.1186/s13036-021-00255-8
[203] L. Polo-Corrales, M. Latorre-Esteves, J.E. Ramirez-Vick, Scaffold design for bone regeneration, J. Nanosci. Nanotechnol. 14 (2014) 15–56, https://doi.org/10.1166/jnn.2014.9127
[204] R.I.M. Asri, W.S.W. Harun, M. Samykano, N.A.C. Lah, S.A.C. Ghani, F. Tarlochan, M.R. Raza, Corrosion and surface modification on biocompatible metals: a review, Mater. Sci. Eng. C 77 (2017) 1261–1274, https://doi.org/10.1016/j.msec.2017.04.102
[205] A. Afzal, Implantable zirconia bioceramics for bone repair and replacement: a chronological review, Mater. Express 4 (2014) 1–12, https://doi.org/10.1166/mex.2014.1148
[206] M.Z. Ibrahim, A.A.D. Sarhan, F. Yusuf, M. Hamdi, Biomedical materials and techniques to improve the tribological, mechanical and biomedical properties of orthopedic implants – a review article, J. Alloy. Compd. 714 (2017) 636–667, https://doi.org/10.1016/j.jallcom.2017.04.231
[207] F. Baino, E. Fiume, Elastic mechanical properties of 45S5-based bioactive glass-ceramic scaffolds, Mater 12 (2019), https://doi.org/10.3390/ma12193244
[208] Britannica, Femur, in: T.E.o. Encyclopaedia (Ed.) Encyclopaedia Britannica, 2020,

[209] L. Jiao, Z.Y. Chua, S.K. Moon, J. Song, G. Bi, H. Zheng, Femtosecond laser produced hydrophobic hierarchical structures on additive manufacturing parts, Nanomaterials 8 (2018), https://doi.org/10.3390/nano8080601
[210] S. Pal, G. Lojen, R. Hudak, V. Rajtukova, T. Brajlih, V. Kokol, I. Drstvenšek, As-fabricated surface morphologies of Ti-6Al-4V samples fabricated by different laser processing parameters in selective laser melting, Addit. Manuf. 33 (2020) 101147, https://doi.org/10.1016/j.addma.2020.101147
[211] Q. Sui, P. Li, K. Wang, X. Yin, L. Liu, Y. Zhang, Q. Zhang, S. Wang, L. Wang, Effect of build orientation on the corrosion behavior and mechanical properties of selective laser melted Ti-6Al-4V, Metals 9 (2019) 976, https://doi.org/10.3390/met9090976
[212] N. Jin, F. Wang, Y. Wang, B. Zhang, H. Cheng, H. Zhang, Failure and energy absorption characteristics of four lattice structures under dynamic loading, Mater. Des. 169 (2019) 107655, https://doi.org/10.1016/j.matdes.2019.107655
[213] N. Kladovasilakis, K. Tsongas, D. Tzetzis, Mechanical and FEA-assisted characterization of fused filament fabricated triply periodic minimal surface structures, J. Compos. Sci. 5 (2021), https://doi.org/10.3390/jcs5020058
[214] Ż.A. Mierzejewska, R. Hudák, J. Sidun, Mechanical properties and microstructure of DMLS Ti6Al4V alloy dedicated to biomedical applications, Materials 12 (2019) 176, https://doi.org/10.3390/ma12010176
[215] P. Hartunian, M. Eshraghi, Effect of build orientation on the microstructure and mechanical properties of selective laser-melted Ti-6Al-4V alloy, J. Manuf. Mater. Process 2 (2018) 69, https://doi.org/10.3390/jmmp2040069
[216] M.F. Sadali, M.Z. Hassan, Influence of selective laser melting scanning speed parameter on the surface morphology, surface roughness, and micropores for manufactured Ti6Al4V parts, (2020) 1–11.https://doi.org/10.1557/jmr.2020.84.
[217] W. Orapiriyakul, P.S. Young, L. Damiati, P.M. Tsimbouri, Antibacterial surface modification of titanium implants in orthopaedics, J. Tissue Eng. 9 (2018), https://doi.org/10.1177/2041731418789838
[218] N. Lin, Q. Liu, J. Zou, D. Li, S. Yuan, Z. Wang, B. Tang, Surface damage mitigation of Ti6Al4V alloy via thermal oxidation for oil and gas exploitation application: characterization of the microstructure and evaluation of the surface performance, RSC Adv. 7 (2017) 13517–13535, https://doi.org/10.1039/c6ra28421c
[219] P. Zhang, Z. Zhang, W. Li, Antibacterial TiO2 coating incorporating silver nanoparticles by microarc oxidation and ion implantation, J. Nanomater. 2013 (2013) 1–8, https://doi.org/10.1155/2013/542878
[221] H. Fan, J. Fu, X. Li, Y. Pei, X. Li, G. Pei, Z. Guo, Implantation of customized 3-D printed titanium prosthesis in limb salvage surgery: a case series and review of the literature, World J. Surg. Oncol. 13 (2015) 308, https://doi.org/10.1186/s12957-015-0723-2
[222] D.J. Cohen, A. Cheng, A. Kahn, M. Aviram, A.J. Whitehead, S.L. Hyzy, R.M. Clohessy, B.D. Boyan, Z. Schwartz, Novel osteogenic Ti-6Al-4V device for restoration of dental function in patients with large bone deficiencies: design, development and implementation, Sci. Rep. 6 (2016) 20493, https://doi.org/10.1038/srep20493
[223] L.E. Murr, Metallurgy principles applied to powder bed fusion 3D printing/additive manufacturing of personalized and optimized metal and alloy biomedical implants: an overview, J. Mater. Res. Technol. 9 (2020) 1087–1103, https://doi.org/10.1016/j.jmrt.2019.12.015
[224] L.E. Murr, S.M. Gaytan, E. Martinez, F. Medina, R.B. Wicker, Next generation orthopaedic implants by additive manufacturing using electron beam melting, Int. J. Biomater. 2012 (2012) 245727, https://doi.org/10.1155/2012/245727